



Technische Universität München

Department of Civil, Geo and Environmental Engineering

Chair of Cartography

Prof. Dr.-Ing. Liqiu Meng

Methodology for evaluation of precision and accuracy of different geometric 3D data acquisition methods

Ana Carolina do Nascimento Melo

Master's thesis

Duration: 01.05.2017 – 14.12.2017

Study Course: Cartography M.Sc.

Supervisor: Dr. –Ing Mathias Jahnke

Drs. Richard Knippers

Dipl. –Ing. Univ Matevz Domajnko

Cooperation: Fraunhofer IGD

2017

STATEMENT OF AUTHORSHIP

Herewith I declare that I am the sole author of the submitted Master's thesis entitled: Methodology for evaluation of precision and accuracy of different geometric 3D data acquisition methods and I have not used any sources other than those listed in the bibliography or identified as references. I further declare that I have not submitted this thesis to any other institution.

Munich, 14 of December 2017

Name and Signature

ACKNOWLEDGEMENTS

This work was developed during my internship as a master thesis writer at the Competence Center Cultural Heritage Digitization (CHD) at Fraunhofer IGD, Darmstadt. At this point, I would like to thank all those who supported and encouraged me during the writing of this thesis as well as in the course of my studies.

First, I would like to thank my supervisor Dipl. –Ing. Univ Matevz Domajnko from Fraunhofer IGD for his guidance, patience and for sharing with me his extensive knowledge. His support and constructive criticism have always been an asset to this work.

I would to express my gratitude to my supervisor Dr. –Ing Mathias Jahnke from TUM for his punctual advices and unreserved support during this work. His comprehension and valuable instructions steered me in the right the direction.

I would also like to acknowledge M.Sc. Inform. Pedro Santos for giving me the opportunity to write my thesis at the CHD department, to Daniel Herb for his support and contribution on my work and to my Hiwi friend Johannes Ball for his insightful advices. Likewise, I thank all other Hiwi colleagues for making this a pleasant experience.

A special thanks to our Programme Coordinator Cartography M.Sc., Juliane Cron. Her kindness and assistance during these past two years goes beyond expected. Her immense support truly makes this experience much more delightful.

Finally, I must express my very profound gratitude to my family and boyfriend for providing me with unfailing support and continuous encouragement throughout these two years and through the process of researching and writing this thesis. This accomplishment would not have been possible without them.

Thank you all!!!

ABSTRACT

3D optical scanning systems have been gaining considerable space in metrology, being largely applied in industry sectors and in the cultural heritage domain. The amount of available sensors on the market has grown considerably. Thereby, deciding for the right technique that *fits-to-a-purpose* or the most cost efficient technology, is a challenging task. When deciding in which technology to invest, the user often relies on the manufacturer's instructions. However, manufacturers generally do not state under which conditions such values were acquired and thus, the system's reproducibility is not assured. If measurements could be traced back to a common standard, this problem could be easily addressed. As such a solution is still not available, specialist often tend to solve this issue by associating terms like precision, accuracy and uncertainty to a measurement. Nowadays, the most applicable solution to define the accuracy of a system relies on the VDI/VDE 2634.

This master thesis aims to develop a common solution to assess accuracy for different geometric 3D data acquisition models, considering the specifications of the VDI/VDE 2634 Part 3. The methodology proposed here encompasses the entire process from the acquisition to its processing stage. The study-case comprehend triangulated methods, as photogrammetry and laser line sensor.

During the acquisition, a calibrated probing body and adapted test are proposed. The processing stage includes a best-fit algorithm and an evaluation of measurement uncertainty. The result comprehends the quality parameters together with the visualization of measurement uncertainty supporting the entire system. Therefore, providing to the end user enough information about the capability of the evaluated system.

Keywords: 3D scanning system, VDI/VDE 2634 Part 3, accuracy, measurement uncertainty, visualization of uncertainty, best-fit algorithm

LIST OF FIGURES

FIGURE 1: SCHEMATIC STRUCTURE OF THE MASTER THESIS	13
FIGURE 2: 3D POINT RECONSTRUCTION BASED ON PLANAR IMAGES (MOONS ET AL. 2008, P. 293)	17
FIGURE 3: BUNDLE ADJUSTMENT APPLICATION (LIMA JULY 10TH, 2006, P. 49).....	17
FIGURE 4: 3D MODEL ACQUISITION WORKFLOW	17
FIGURE 5: IMAGE ACQUISITION DEPICTION USED FOR THE SFM (WESTOBY ET AL. 2012, P. 301)	19
FIGURE 6: LASER LINE PRINCIPLE (BLAIS 2004, P. 234)	20
FIGURE 7: DIFFERENT POSITIONS OF THE SENSOR RELATED TO THE SPHERE POSITION (ACKO ET AL. 2012, P.04)	22
FIGURE 8: POSITION OF A SPHERE WITHIN THE SENSOR MEASURING VOLUME (ACKO ET AL. 2012, P.04)	22
FIGURE 9: PROPOSED ARRANGEMENT FOR THE ACQUISITION OF THE SPHERE SPACING ERROR (ACKO ET AL. 2012, P.04).....	23
FIGURE 10: METHODOLOGY OVERVIEW.....	34
FIGURE 11: SKETCH OF THE SPHERES PLATES CREATED IN SKETCHUP	35
FIGURE 12: COATING INDICATION	37
FIGURE 13: COATING EVALUATION PERFORMED IN CLOUDCOMPARE	37
FIGURE 14: SPHERE PLATE BEFORE AND AFTER ITS PREPARATION.....	38
FIGURE 15: DEFINED POSITIONS FOR THE SD ACQUISITION	39
FIGURE 16: BEST-FIT ALGORITHM STEPS	41
FIGURE 17: RADIAL DISPERSION VISUALIZATION FOR EACH EVALUATED SCAN SYSTEMS (GENERATED WITH MATLAB).....	57
FIGURE 18: PS EVALUATION BASED ON THE MEAN VALUE, CREATED WITH MATLAB.....	58
FIGURE 19: SD EVALUATION OF EACH POSITION FOR THE NIKON D610 WITH AF-S NIKKOR 50MM LENS (CREATED WITH MATLAB).....	59
FIGURE 20: SD EVALUATION FOR EACH POSITION OF THE LASER LINE SCANNER, CREATED WITH MATLAB.....	60
FIGURE 21: SD EVALUATION FOR EACH POSITION OF THE NIKON D610 WITH AF-S NIKKOR 50MM LENS, CREATED WITH MATLAB	60
FIGURE 22: SD EVALUATION FOR EACH POSITION OF THE CANON 5DSR + CANON 100MM LENS, CREATED WITH MATLAB	61
FIGURE 23: SENSOR MEASURING OF THE SYSTEMS UNDER TEST VOLUME (OPENGL PERFORMER) ...	68

LIST OF TABLES

TABLE 1: CANON 5DSR + CANON 100MM LENS SETTINGS OVERVIEW	30
TABLE 2: NIKON D610 + AF-S NIKKOR 50MM LENS SETTINGS OVERVIEW	30
TABLE 3: SENSOR MEASURING VOLUME OF THE EVALUATED SCANNING SYSTEMS.....	32
TABLE 4: MEASUREMENT VOLUME OF THE EVALUATED SCAN SYSTEMS	32
TABLE 5: SPHERE SPECIFICATIONS ACCORDING TO THE DIN 5401 (RGPBALLS 2017).....	35
TABLE 6: PLATE SPECIFICATIONS ACCORDING TO THE SPECIFICATIONS OF THE MANUFACTURER ..	36
TABLE 7: CALIBRATION VALUES ACCORDING TO DIN 5401 (RGPBALLS 2017)	47
TABLE 8: PROBING ERROR ANALYSIS	50
TABLE 9: SPHERE SPACING AND LENGTH MEASUREMENT ERROR ANALYSIS	51
TABLE 10: STANDARD UNCERTAINTY PROBING ERROR	52
TABLE 11: STANDARD UNCERTAINTY SPHERE SPACING ERROR (70MM SPHERE)	52
TABLE 12: STANDARD UNCERTAINTY SPHERE SPACING ERROR (38MM SPHERE)	52
TABLE 13: UNCERTAINTY BUDGET USING PF ACQUIRED FROM THE PHOTOGRAMMETRIC SYSTEM II	53

ABBREVIATIONS

BIPM	International Bureau of Weights and Measure
CHD	Cultural Heritage Digitization
CMM	Coordinate Measuring Machine
E	Length Measurement Error
FOV	Field of View
GMA	Gesellschaft Mess- und Automatisierungstechnik
GUM	Guide to the Expression of Uncertainty in Measurement
IGD	Institute for Computer Graphics Research
k	coverage factor
MPE	Maximum Permissible Error
PF	Probing Error Form
PS	Probing Error Size
SD	Sphere Spacing Error
u	Standard uncertainty
U	Expanded uncertainty
VDI	Verein Deutscher Ingenieure
VDE	Verband der Elektrotechnik, Elektronik und Informationstechnik
SfM	Structure from Motion
SIFT	Scale Invariant Feature Transform

TABLE OF CONTENTS

1	INTRODUCTION.....	11
1.1	MOTIVATION AND PROBLEM STATEMENT	11
1.2	RESEARCH OBJECTIVES	12
1.3	RESEARCH QUESTIONS	12
1.4	THESIS STRUCTURE	12
2	THEORETICAL BACKGROUND	14
2.1	ACCURACY ASSESSMENT	14
2.1.1	Related Work.....	14
2.1.2	Triangulated Scanning Systems Overview	16
2.1.3	VDI/VDE 2634	20
2.1.4	VDI/VDE 2634 Part 3	20
2.2	MEASUREMENT ERROR AND MEASUREMENT UNCERTAINTY	23
2.2.1	Systematic and random measurement errors.....	24
2.2.2	Measurement Uncertainty	24
2.2.3	Test Procedure Uncertainty	26
2.3	VISUALIZATION OF MEASUREMENT UNCERTAINTY	27
2.3.1	Related Work.....	27
3	STUDY CASE.....	30
3.1	Cultural Heritage Digitization (CHD)	30
3.1.1	Equipment characteristics	30
3.1.2	Laser Line System.....	31
3.1.3	Sensor Measuring Volume and Measurement Volume.....	31
3.1.4	Experiment setup.....	32
4	METHODOLOGY	34
4.1	WORKFLOW.....	34
4.2	INPUT PREPARATION	34
4.2.1	Artefact design	34
4.2.2	Artefact preparation.....	36
4.3	Adapted tests.....	38
4.3.1	Probing Error test	38
4.3.2	Sphere Spacing Error test	39
4.3.3	Length Measurement Error test.....	40
4.4	Point cloud acquisition	40

4.5	Best-fit algorithm.....	40
4.5.1	Assumption.....	40
4.5.2	Algorithm Framework.....	41
4.5.3	Sphere Fit	41
4.5.4	Radial error.....	42
4.5.5	Minimization	43
4.6	Evaluation and assessment of the adapted tests.....	44
4.6.1	Assumption.....	44
4.6.2	Evaluation of the adapted tests.....	44
4.6.3	Assessment test	46
4.7	Measurement uncertainty evaluation.....	46
4.7.1	Assumption.....	46
4.8	Online Survey	49
4.9	Software used	49
5	RESULTS AND DISCUSSION.....	50
5.1	Accuracy results	50
5.1.1	Probing Error analysis.....	50
5.1.2	Sphere-Spacing Error and Length Measurement Error analysis.....	51
5.2	Measurement uncertainty results	52
5.2.1	Test procedure results.....	52
5.2.2	Measurement uncertainty analysis	53
5.3	Online survey results	53
5.3.1	Part I analysis	54
5.3.2	Part II analysis.....	54
5.3.3	Part III analysis.....	55
5.3.4	Overall analysis	55
5.4	Measurement uncertainty visualization results.....	55
5.4.1	Probing Error Form visualization.....	55
5.4.2	Probing Error Size visualization	56
5.4.3	Sphere Spacing Error visualization	59
6	CONCLUSION AND FURTHER WORK	62
	BIBLIOGRAPHY	64
	APPENDIX.....	68
A	Sensor Measuring Volume and Measurement Volume.....	68

a.	Sensor Measuring Volume	68
b.	Measurement volume	69
B	Best-fit algorithm and Script	70
a.	sphereFit function	70
b.	Radial error function.....	70
c.	Minimization	71
d.	Script.....	74
C	Accuracy analysis – evaluated scan systems.....	79
a.	Accuracy analysis – Laser Line Scanner System	79
b.	Accuracy analysis– Photogrammetric System I.....	80
c.	Accuracy analysis – Photogrammetric System II.....	81
D	Measurement uncertainty analysis	82
a.	Uncertainty Budget – Laser Line Scanner System.....	82
b.	Uncertainty Budget – Photogrammetric System I.....	83
c.	Uncertainty Budget – Photogrammetric System II	84

1 INTRODUCTION

1.1 MOTIVATION AND PROBLEM STATEMENT

3D imaging systems have become more accessible to innumerable fields of application, as in Geomatics and Cultural Heritage domain (Beraldin et al. 2012). 3D imaging systems can be classified as time-of-flight, interferometer and triangulation methods. With triangulation method being largely applied nowadays, several users have been venturing themselves without much or prior knowledge of the evaluation and methodology behind the technique (Beraldin et al. 2007a). According to Beraldin et al. (2007a, p. 04) „ In order to take full advantage of 3D imaging systems, one must understand not only their advantages but also their limitations.“.

An appropriate method to understand system applicability and capability relies on assessing its accuracy and uncertainty. These values can be acquired by tracing the measurement back to a standard (Beraldin et al. 2007a). When compared to other optical distance measurements, optical 3D imaging systems are relatively new and no official standard for its evaluation is available. Thus, according to Beraldin et al. (2015) without an international standard the user will hardly be certain about the system's performance. Hence, choosing between optical 3D imaging system, will continue to be challenging (Barbero, Ureta 2011). According to Mendricky (2016, p. 1571) the VDI/VDE 2634 guideline „[...] is currently the only general recommendation on how to evaluate accuracy of optical systems.“

The VDI/VDE 2634 Part 3 evaluate systems operating with triangulation principle (Beraldin et al. 2015; VDI/VDE 2634 Part 3 2008). The guideline provides a methodology to determine the quality of the system through appropriate parameters and physical standards (Beraldin et al. 2015). These parameters assess the accuracy of the system and are defined as Probing Error Form (PF), Probing Error Size (PS), Sphere Spacing Error (SD) and Length Measurement Error (E). While, the physical standards refers to the calibrated object used for the system evaluation. The guideline refers to the calibrated objects as *artefact* (VDI/VDE 2634 Part 3 2008).

The term *accuracy* express the difference between the measured data and the *true value*¹ (NDT Resource Center n.d). Once the result from any measurement will never be an absolute value, the true value of an observation cannot be acquired. (Luhmann et al. 2014; Pöthkow, Hege 2011; Stadek 2015). Thereby when handling measured or generated data, the uncertainty must always be incorporated to it (Bonneau et al. 2014; Brodlie et al. 2012; Sanyal et al. 2009; Pöthkow, Hege 2011; Grigoryan, Rheingans 2004; Pöthkow, Hege 2011).

Hence when data are used for visualization purposes, the uncertainty associated to the data should also be incorporated to its representation (Brodlie et al. 2012; Zhang et al. 2017; Pang et al. 1996). Portraying uncertainty is not a simple task once every uncertainty carries a certain degree of complexity (Brodlie et al. 2012). However its visualization should support decision-making (Bonneau

¹In any measurement application, true value cannot be establish or acquired. Thus physical standards used as reference are employed as true value (NDT Resource Center n.d).

et al. 2014; Grigoryan, Rheingans 2004) and thus, provide a „non-distracting“ representation (Grigoryan, Rheingans 2004, p. 01).

This master thesis will address the concepts above related to assess the accuracy and visualize the uncertainties for optical 3D scan systems. A general solution was developed following the VDI/VDE 2634 Part 3 specifications and will be applied to the study case of this master thesis. Thus, the accuracy of optical 3D scanning systems developed at the Fraunhofer Institute for Computer Graphics Research (IGD) and the visualization for the uncertainties associated to the data will be evaluated.

The Competence Center Cultural Heritage Digitization (CHD) at Fraunhofer IGD has developed, over the years, scanning technologies in order to improve their work with 3D digitization of cultural heritage objects. The scanning technologies developed by the department includes photogrammetry and structure-light scanner. Therefore, to contribute with the department’s research, this master thesis will evaluate three equipment: Nikon D610 with AF-S Nikkor 50mm lens, Canon 5DSr with Sigma 100mm lens and a laser line scanner.

1.2 RESEARCH OBJECTIVES

The overall objective of this research is to create a methodology to assess the accuracy for optical 3D scan systems as well as to provide the visualization of the uncertainties in order to support the results. The aim is to develop a general solution considering the specifications of the VDI/VDE 2634 Part 3 which could be applied to any scan system that complies with the guideline. Following this general solution, the user will be able to generate the results for the certificate of accuracy with the visualization of the measurement uncertainty supporting it. Thus, providing to the final user enough information about the evaluated system, assisting in the decision-making.

1.3 RESEARCH QUESTIONS

In order to meet the main objective of this work, the following research questions should be addressed:

- How to prepare the artefact²?
- How to evaluate and compute each quality parameter?
- Which uncertainties can be accounted?
- How these uncertainties can benefit the user?
- How to visualize the association of accuracy + uncertainties for each quality parameter?

1.4 THESIS STRUCTURE

This master thesis encompass two main subjects, the accuracy assessment and the visualization of uncertainty. Although they can be analyzed as two distinct parts, the domains are complementary. Thus, the parameters that represent the quality of each scan will be then used in the visualization of uncertainty.

² In this master thesis as well as in the VDI/VDE 2634 Part 3, calibrated objects are referred as artefact.

The work developed in this master thesis is structured in six chapters, as illustrated in Figure 1.



Figure 1: Schematic structure of the master thesis

In the first chapter, a brief introduction of the motivation and problem statement is described. In addition, the research objectives are presented as well as, the research questions that need to be addressed to acquire it. The second chapter is the theoretical background and related work. In this chapter, a brief background of the concepts and methods used is provide to the user. The third chapter introduces the study case, where a brief overview of the application is provided. The fourth chapter covers the research development methodology. It starts with a workflow followed by input preparation. Then, the adapted test and the best-fit algorithm are described followed by the presentation of the evaluated uncertainty and the online survey. In the fifth chapter, the results and discussion of the accuracy and visualization are analyzed. Conclusion and further work is then provided in the last chapter of this research.

2 THEORETICAL BACKGROUND

In this chapter, it is provided an overview of how the research objectives can be met to generate a broad solution for the assessment of the accuracy for optical 3D scanning systems. To compose the solution, it is necessary to partition the related concepts: accuracy assessment and the visualization of measurement uncertainty, and analyze them individually.

Thus, in the first part a related work from the methods applied to assess accuracy for different scan systems is introduced. Based on the related work and the aim of this research, a brief overview regarding the sciences behind the technologies and a summary of the employed guideline is provided. In order to justify the use of assessment of accuracy with visualization of uncertainties on the measurement, a section named Measurement Error and Measurement Uncertainty in between both criteria is introduced. The aim is to establish a clear connection between both concepts and make it easier for the user to perceive the reasons why these concepts are being related. The Chapter ends with the visualization of measurement uncertainty. A brief overview regarding the benefits the visualization of the uncertainty in the data can provide followed by the related work.

2.1 ACCURACY ASSESSMENT³

2.1.1 Related Work

With the growing application of non-contact 3D scan systems in metrology, different studies trying to assess their accuracy using standards and guidelines or not have been released.

Barbero, Ureta (2011) compared five different scan systems in their article, in order to assess the quality and accuracy of them. The quality was assessed through the analysis of the mesh and point distribution, while the accuracy was achieved by comparing the measurement results to the calibration certificate of the objects. Objects such as spheres, cylinders and gauge blocks were used for the accuracy assessment. The work also evaluated the uncertainty of the measurement by using the ISO 15330-3.

Guidi et al. (2010) evaluate seven different 3D ranging sensors for accuracy, uncertainty and resolution. For the accuracy part, the authors account for the systematic error by evaluating the linear, angular and relative linear accuracy. The linear and angular accuracy were obtained by the comparing deviation between the best-fit geometry of the measured object to the ground truth. While the relative linear accuracy evaluated the point cloud for its theoretical position to the diagonal of the range map.

Carmignato, Savio (2011) evaluated the probing error and the length measurement error for coordinate measuring systems with optical distance sensors using a VDI guideline, the VDI/VDE 2617-6.2. Calibrated objects were employed during the system's performance. The authors pointed to the necessity of preparing the calibrated objects in order to avoid influence of the objects properties

³ In this master thesis as well as in the VDI/VDE 2634 Part 3, the word *evaluation* is used during the analysis of the quality parameters. While the word *assessment* is used to state that, the results of each quality parameter have been accepted.

when assessing the accuracy of the system. Thus, the authors also evaluated different materials and surface treatment.

Acko et al. (2012) propose in their study three different artefacts to test measurement capability and calibration of different types of Coordinate Measuring Machines (CMMs). The tetrahedron developed in their study comply with existing guidelines, as the VDI/VDE 2634 Part 2 and Part 3, being suitable for fringe projection and other related 3D scan assessment applications.

Beraldin et al. (2015) presents a summary of existing standards to evaluate accuracy of 3D measurement system, varying from micro to long range. For close range application, defined in the article as measurement made within 10mm to 2m distance, several standards with a bigger focus on the ISO 10360-8 and the VDI/VDE 2634 guideline was provided. The authors also addressed a discussion regarding physical standards used in the evaluation of the accuracy in close range applications.

Mendricky (2016) assessed the accuracy of an optical measurement system, the ATOS 3D optical scanner. The acceptance test was performed with an etalon plate designed to evaluate three different volume measurements of the scanner. Although the test was performed according to specification provided by the manufacturer, GOM, this was in accordance to the VDI/VDE 2634 Part 3.

Sims-Waterhouse et al. (2017), used micro-scale object to evaluate the accuracy of a photogrammetric device. The Probing Error and Sphere Spacing Error were tested based on the VDI/VDE 2634 Part 3, with a few modifications applied to it. Thus, a different configuration for the object tested for the SD was created and some adaptations based on the ISO 10360 Part 8 were also included.

Non-contact optical 3D scan systems have been largely applied on metrology (Beraldin et al. 2012), even though considered a new technology (Beraldin et al. 2015). Thus, based on the above related work and industry application, a 3D scanning and photogrammetry system will be applied to the common solution proposed by this master thesis. The 3D scanning choice can be justified since it is „Among the most widely used in the industry, the laser optical system obtains the points very rapidly by triangulation;“ as mentioned by Barbero, Ureta ((2011, p. 189) . While the photogrammetric system is considered „[...] very simple technique in practice.“ (Sims-Waterhouse et al. 2017, p. 02) where the measurements are not easily disturbed by external conditions (Lima July 10th, 2006).

To provide more traceability to the proposed solution, the tests will be evaluated based on the VDI/VDE 2634 Part 3. As there is still no available international standards to provide accuracy for non-contact optical systems (Beraldin et al. 2012) and being the VDI/VDE 2634 Part 3 not only the most accepted recommendation for optical 3D scanning systems (Mendricky 2016) but also the only one applicable to photogrammetric systems (Sims-Waterhouse et al. 2017).

The work in this master thesis will differ from the above related work since a general solution for the assessment of the accuracy for different optical 3D scanning systems based only on the VDI/VDE 2634 Part 3 guideline is provided.

2.1.2 Triangulated Scanning Systems Overview

The following sub-sections will introduce a brief overview of the chosen scanning systems. As this master thesis will use the VDI/VDE 2634 Part 3 as a base to establish a general solution for the assessment of the accuracy, close-range photogrammetry and 3D scanning systems will be described in this chapter.

It is important to mention that triangulated 3D scan systems have a relatively small volume of measurement if compared to other scan systems, as time-of-flight (Beraldin et al. 2012). Volume of measurement define the area/size of the measured (SMARTTECH 3D scanners n.d; VDI/VDE 2634 Part 3 2008), and this is why close-range photogrammetry is addressed in this master thesis.

2.1.2.1 Close-range Photogrammetry

Photogrammetry⁴ is gaining considerable space in close-range measurement due to its low financial investment, if compared to other 3D scan techniques, applicability to inaccessible areas measurement, simple operation and easy measurement acquisition (Yilmaz et al. 2007; Lerma et al. 2010; Sims-Waterhouse et al. 2017).

Close-range photogrammetry or terrestrial photogrammetry⁵ is applied to the measurements executed from at most 300m distance between the sensor and the object (Matthews 2008, p. 11; Luhmann et al. 2014).

In Close-range photogrammetry as well as in Photogrammetry, the input is always an image. From this input, outputs like maps, different drawings, measurements and point cloud can be acquired (Luhmann et al. 2014).

Close-range photogrammetry uses a central perspective projection (convergent acquisition) when capturing the images (Liu, Huang 2016; Luhmann et al. 2014; Yilmaz et al. 2007). Planar images cannot contain the same level of detail as a 3D model, therefore, during the acquisition process some information is suppressed, as depth perception (Geodetic Systems n.d; Luhmann et al. 2014). Thus, for the reconstruction two or more images with a good overlapping area are recommended (Geodetic Systems n.d).

Photogrammetry uses the triangulation principle to retrieve information from a 2D image to reconstruct and generate objects in the 3D space. When the camera poses and the homologous points are known, it is possible to reconstruct the rays and find the position of the point in a 3D space, as represented in Figure 2 (Geodetic Systems n.d; Moons et al. 2008).

⁴ The word Photogrammetry in this research refer to image-based 3D reconstruction.

⁵ In this master thesis, close-range photogrammetry will be employed to address the science.

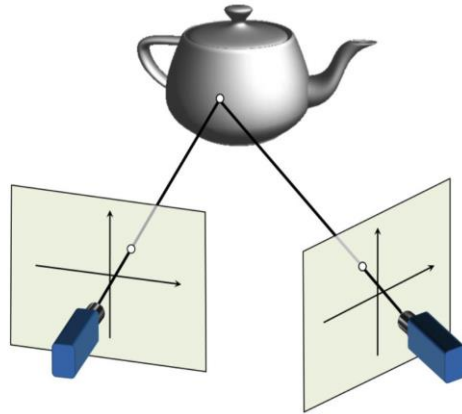


Figure 2: 3D point reconstruction based on planar images (Moons et al. 2008, p. 293)

When more than one point in each image is forward intersected, the bundle of rays generate a *bundle triangulation*. This method uses triangulation together with bundle adjustment to acquire the image orientation and provide the 3D coordinate with higher trust (Luhmann et al. 2014). Figure 3 provides an illustration of the bundle adjustment applied to 2D images to reconstruct the 3D model.

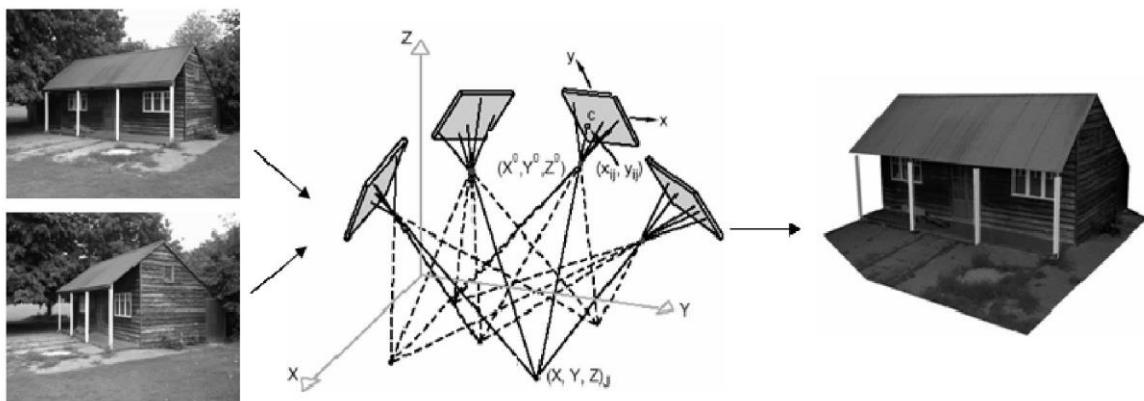


Figure 3: Bundle adjustment application (Lima July 10th, 2006, p. 49)

A generally applied workflow in close range photogrammetry for the acquisition of the 3D model, consists of:



Figure 4: 3D model acquisition workflow

Being camera calibration and image 3D reconstruction important steps that can influence on the final 3D model, a small explanation about the concepts is provided below.

2.1.2.1.1 Camera calibration

Camera calibration is a fundamental step in image-based 3D reconstruction when an accurate model is aimed (Joshi 2014). In photogrammetry, camera calibration is used to define the intrinsic

parameters⁶ of the camera, focal length and principle point, as well as the necessary correction of the distortions, mostly radial and tangential (Luhmann et al. 2014).

Distortion of the lens can be described by how the light rays bend the image plane and by the orientation of the image plane related to the sensor lens. Thus, by finding the radial and tangential optical distortion coefficient, the distortion of the lens can be corrected (MathWorks 2017). After correcting the distortions and identifying the intrinsic parameters, the camera is said to be calibrated (Luhmann et al. 2014). Thus, camera calibration is applied to have at the end an image model similar to the one acquired by a pin-hole camera (Joshi 2014).

The process for camera calibration uses, normally, bundle adjustment and thus, extrinsic parameters⁷ and metric values can also be estimated in this step (Luhmann et al. 2014).

According to Joshi 2014), the image center, „[...]the “focus” of the camera [...]“, the skew coefficient, the image scale and the „[...]pseudo zoom effect [...]near the center of any image. “, are camera parameters and settings influenced during the image acquisition. Thus, after calibration parameters are defined, it is important to keep camera setting constant so the calibration parameters are not voided (Luhmann et al. 2014).

2.1.2.1.2 Image-based 3D reconstruction

With image-based 3D reconstruction being largely applied nowadays, the traditional techniques of photogrammetric is being replaced by an automatic solution where the reconstruction does not require a prior knowledge of camera poses and known coordinates. This process is named *Structure from Motion - SfM* (Snavely 2008).

The general acquisition of images used in SfM process consists of several images taken around the object with distinct camera poses that ensures a good overlapping area, as illustrated in Figure 5 (Westoby et al. 2012; Agisoft LLC 2017). According to Snavely (2008), during the processing phase the problem can be split into two parts: feature and camera pose detection. The first one can be solved by algorithms like SIFT (Westoby et al. 2012), while the second one will be solved by the matched features obtained in the first part. With multiple matched points, the camera poses can be estimated and thus, the 3D coordinate can be assessed through triangulation. „The problem of using pixel correspondences to determine camera and point geometry in this manner is known as SfM. “ (Snavely 2008).

According to Moons et al. (2008), as SfM acquires multiple images of the objects, self-calibration is applied instead of normal calibration. However, when the probing body is not very representative in the image frame, self-calibration is generally not representative (Beraldin et al. 2007b) and thus, camera calibration is necessary.

⁶ Intrinsic parameters are defined by the interior orientation of the camera (focal length and principle point) and the skew coefficient (MathWorks 2017).

⁷ Extrinsic parameters, or exterior orientation, describes the location and orientation of the camera in the 3D space (MathWorks 2017).

The major advantage of self-calibration is that the method uses the acquired images, to extract the intrinsic and extrinsic parameters (Luhmann et al. 2014; Moons et al. 2008). Thus, during the bundle adjustment step, the calibration parameters and camera poses are extracted jointly with the final model reconstruction (Luhmann et al. 2014).

The output generated from SfM is, normally, unscaled (Geodetic Systems n.d; Westoby et al. 2012). Without a known coordinate system or a metric value during the reconstruction, it will not be possible to acquire the object dimensions (Lima July 10th, 2006). Therefore, it is a common practice to display identifiable targets, normally with a high contrast, in the scene previous to the image acquisition (Lima July 10th, 2006; Westoby et al. 2012). This approach has also advantages over the registration and bundle adjustment executed in the SfM (Westoby et al. 2012).

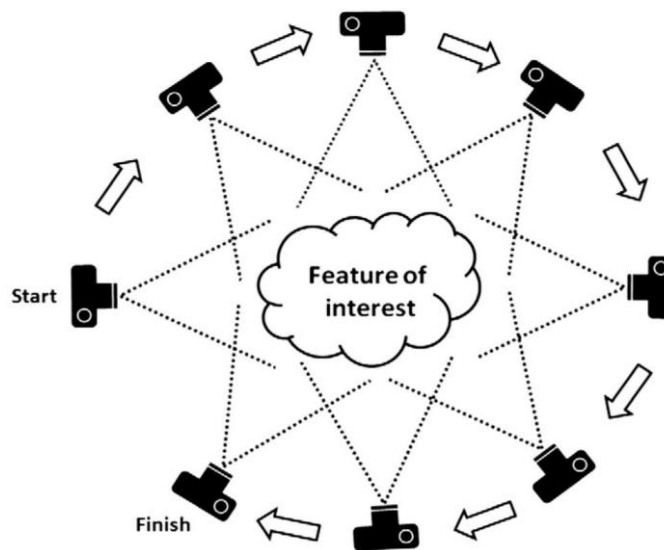


Figure 5: Image acquisition depiction used for the SfM (Westoby et al. 2012, p. 301)

2.1.2.1.3 3D scanning systems

3D scanning based on triangulated system has gained considerable investments over the past years and thus, has become a widely accepted technology for metrology. Among the available ranging sensors, the laser line is the most used due to its simplicity and cost efficiency (Blais 2004).

Different from the photogrammetric principle, 3D scanning systems are an active technology (Beraldin et al. 2012). One way of active triangulation system is by projecting a laser line on the object, and the camera sensor coupled to it captures the image (Barbero, Ureta 2011; Guidi et al. 2010). The sensor then, estimates the 3D position through the deformation of the incident light on the object (Blais 2004). These positions however are inherent to the sensor coordinates and thus, it is necessary to convert them to local coordinates. According to Bernardini, Rushmeier (2002, p. 150), the 3D coordinate can be acquired by „using the calibrated position and orientation of the light source and sensor .“. Figure 6 illustrates this entire description.

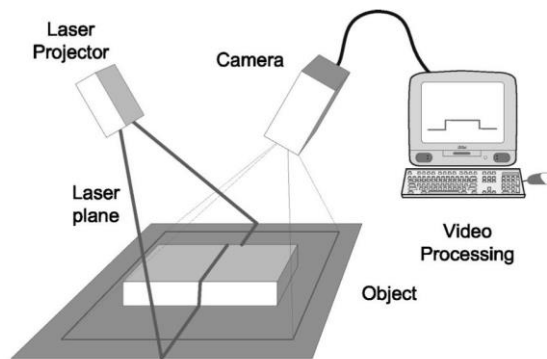


Figure 6: Laser line principle (Blais 2004, p. 234)

To generate the 3D model, the laser line scanner normally makes use of mechanical motion that allows the complete acquisition of the object (Blais 2004).

2.1.3 VDI/VDE 2634

With the growth of optical 3D scanning systems application in metrology, it became more and more evident the need of a common standard for assessing the system's accuracy. A standard that depicts system applicability, support in the interpretation of the quality achieved by the manufacturer and therefore, aid the user to decide among optical scan systems (Beraldin et al. 2012, pp. 53–54).

According to Beraldin et al. (2015), it is in this scenario that the VDI/VDE Gesellschaft Mess- und Automatisierungstechnik (GMA) arises establishing acceptance and re-verification test in order to assess the precision and accuracy of an evaluated system.

The VDI/VDE GMA is an association between German engineers, electronic and information technologies responsible for the development of standards in metrology (Beraldin et al. 2015; VDI 2017). According to Beraldin et al. (2012), the VDI/VDE 2634 descends from an ISO standard and therefore, its quality parameters has analogous principles to CMM systems.

The VDI/VDE 2634 is divided in three parts:

- Part 1 – Imaging systems with point-by-point probing;
- Part 2 – Optical systems based on area scanning;
- Part 3 – Multiple view systems based on area scanning.

The Part 2 and Part 3 of the guideline were created to test area-scanning systems that operate based on the triangulation principle. Part 2 of the guideline is applicable for single images while, the Part 3 for multiple images (VDI/VDE 2634 Part 3 2008). Due to the specifications of the guideline and the limitations of the equipment being tested, only the third part will be addressed in this research.

2.1.4 VDI/VDE 2634 Part 3

In this part of the guideline multiple-area scan is applied to capture the object. The aim is to scan the object in its full. Therefore, any combination between sensor and object, which enables the

reconstruction, can be used. By capturing multiple views, the proposed test also checks how the system is influenced (VDI/VDE 2634 Part 3 2008; Beraldin et al. 2012; Luhmann et al. 2014).

For the acceptance and re-verification tests, the guidelines suggest calibrated artifacts, which has a simple geometric form. (VDI/VDE 2634 Part 3 2008; Acko et al. 2012).

The manufacturer states all the necessary conditions for the acquisition of the results. This includes the material used to manufacture the object, the system set-up and the external conditions under which the parameters were acquired (VDI/VDE 2634 Part 3 2008).

To assess the accuracy of the measuring system the guideline defines three quality parameters:

- Probing Error;
- Sphere Spacing Error;
- Length Measurement Error.

This research will follow the recommendations for the acceptance test. Thus, according to the Beraldin et al. (2012) and the VDI/VDE 2634 Part 3, the parameters named above are only valid after being compared to:

$$|MPE_{xx}| - U \quad (1)$$

where, MPE_{xx} (Maximum permissible error) is stated by the manufacturer (Mendricky 2016); and U is defined in by Formula (6) or (7), depending on the parameter under testing.

The guideline does not account for data filtering, unless these are part from the equipment processing. Thus, for outliers removal the guideline allows at most three out of one thousand points to be removed (VDI/VDE 2634 Part 3 2008).

Below a summary of these quality parameters is presented, however, for further details please refer to the VDI/VDE 2634 Part 3.

2.1.4.1 Probing Error

„The probing error parameter describes the error effects associated with surface point coordinates in a small measurement volume.“ (Luhmann et al. 2014, p. 565)

The Probing Error described in the guideline is evaluated in two parts: the Probing Error Form (PF) and the Probing Error Size (PS). The Probing Error Form (PF) comprehends the radial deviation of the measured points to its theoretical surface, the best-fit sphere (Luhmann et al. 2014; Sims-Waterhouse et al. 2017; VDI/VDE 2634 Part 3 2008). While, the Probing Error Size (PS) is the difference between the diameter of the fitted spheres and the calibrated sphere. The fitted sphere is calculated by the least square method with free radius (VDI/VDE 2634 Part 3 2008).

The analyzed surface is a sphere where, its dimensions are in accordance to spatial diagonal of the sensor's measuring volume being tested (VDI/VDE 2634 Part 3 2008).

For the acquisition of the Probing Error, it is suggested that the sphere should be captured from at least three different positions in the measuring volume (Figure 7). Where for each chosen position of the sphere, a minimum of five image/cloud should be used for the reconstruction (Beraldin et al. 2015; VDI/VDE 2634 Part 3 2008). Moreover, it has been also suggested that the sphere should be located in different positions within the sensor measuring volume (Figure 8), for the each defined positions of the sensor (VDI/VDE 2634 Part 3 2008).

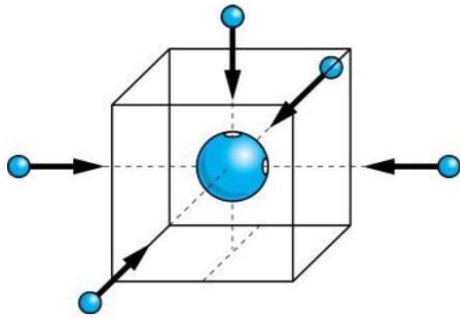


Figure 7: Different positions of the sensor related to the sphere position (Acko et al. 2012, p.04)

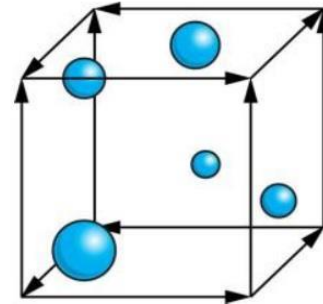


Figure 8: Position of a sphere within the sensor measuring volume (Acko et al. 2012, p.04)

2.1.4.2 Sphere Spacing Error

The quality parameter Sphere Spacing Error (SD) defines the length in between the centers of two spheres and compares it to the calibrated length, in order to define the system's deviation (VDI/VDE 2634 Part 3 2008; Mendricky 2016; Sims-Waterhouse et al. 2017, 2017).

The SD quality parameter is achieved by calculating the Euclidian distance from the centers and then, subtracting the measured length from the calibrated length. Where, the center point of each sphere is acquired through the least-square method with variable radius (VDI/VDE 2634 Part 3 2008; Luhmann et al. 2014).

For measuring the SD, objects having two spheres with a certain distance in between are employed (Beraldin et al. 2015). According to VDI/VDE 2634 Part 3, the spheres are designed based on the spatial diagonal of the sensor's measuring volume of the tested equipment. While the length in between the spheres is in accordance to the body diagonal of the measuring volume of the evaluated optical 3D scan system.

The guideline also suggest a configuration to assess the quality parameter SD using the above described artefact as illustrated by Figure 9 (VDI/VDE 2634 Part 3 2008; Acko et al. 2012).

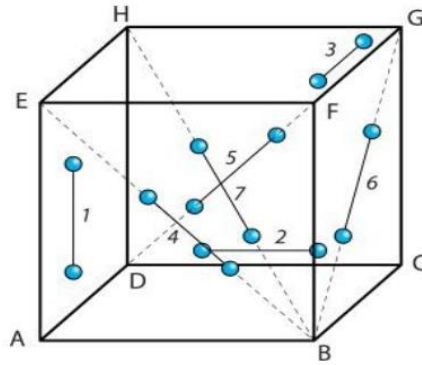


Figure 9: Proposed arrangement for the acquisition of the sphere spacing error (Acko et al. 2012, p.04)

2.1.4.3 Length Measurement Error

„The length measurement error is used to analyze the accuracy of length measurement“ (Luhmann et al. 2014, p. 560).

The length measurement error (E) is defined in the DIN EN ISO 10360 and considers the effects of the probing error. Thus, E is defined as the measurement of the length between two outer points, located at each end of the measured length (VDI/VDE 2634 Part 3 2008; Carmignato, Savio 2011; Beraldin et al. 2015).

The artefact proposed for determining E, can be analogous to the artefact proposed for the SD (VDI/VDE 2634 Part 3 2008; Beraldin et al. 2015).

According to the VDI/VDE 2634 Part 3, three methods are available to calculate the quality parameter. Thus, the manufacturer should state which method to use for the calculation of E.

2.2 MEASUREMENT ERROR AND MEASUREMENT UNCERTAINTY

The International Bureau of Weights and Measure (BIPM) defines accuracy as the closest approximation between measured value and the *true value*. (NDT Resource Center n.d; BIPM 2008). As the acquisition of the true value is not feasible in reality, often a ground truth value associated to an ISO standard is used to replace it (NDT Resource Center n.d). In this research, the ground truth refers to the calibrated artefact. Accuracy is a theoretical value and cannot be measured, therefore its analysis is made through the measurement error (BIPM 2008), here given by the quality parameters.

The measurement error encompass systematic and random error and does not account for mistakes introduced in the measurement (NDT Resource Center n.d; BIPM 2008). Both terms will be addressed more in details in the following sub-section.

Uncertainty by its turns, defines the interval where true value can be encountered (NDT Resource Center n.d). Uncertainty accounts for different components that can influence on the measurement. However, when uncertainty is associated to the measurement it gives higher trust to the measurement,

aiding in a better comprehension of the measurand⁸ value and the causes that affect it (Ball 2014). Uncertainty is also being addressed more in details in this section.

The above concepts constitute the basis of this research where accuracy and measurement error are used in the first phase and uncertainty will be covered in the second phase, when the visualization of the uncertainty associated to the measurement will be addressed.

2.2.1 Systematic and random measurement errors

Every measurement carries errors arising from the measuring process. These can be introduced as systematic errors and/or random errors. Systematic errors, as the name suggests, introduces in the measurement a systematic error behavior in the same direction (i.e. adding on the observation) or they follow a certain rule. These errors can be eliminated from the measurement through calibration techniques and repeated observations. When systematic errors cannot be corrected, they are introduced in the measurement as random errors. Random errors do not have a pattern behavior and they cannot be precisely modeled. Therefore, each measurement will carry at least, the random error (Luhmann et al. 2014; Stadek 2015; Pöthkow, Hege 2011).

2.2.2 Measurement Uncertainty

The International Bureau of Weights and Measures (BIPM) define measurement uncertainty as „ non-negative parameter characterizing the dispersion of the quantity values being attributed to a measurand, based on the information used “ (BIPM 2008, p. 25).

As explained above, measurements will never return the true value for the measurement observations. Therefore, in order to introduce more confiability to the measurement, the measurement uncertainty should be specified (Luhmann et al. 2014; Stadek 2015).

According to Luhmann et al. (2014) and Stadek (2015), measurement (X_o) and measurement uncertainty (U) are normally defined by the following formula:

$$X_o \pm U, \tag{2}$$

As it is not certain the magnitude of the uncertainty over the observations, a coverage factor k^9 is introduced (Luhmann et al. 2014, p. 553). When the uncertainty is defined as *standard uncertainty* (u), it is expressed as the standard deviation of the measurement and use $k = 1$. For k values above 1, the uncertainty is defined as *expanded uncertainty* (U) and it refers to the confidence interval used to define the measurement (Luhmann et al. 2014; Stadek 2015; JCGM 2008). U is normally given by the following formula:

$$U = k \cdot u \tag{3}$$

⁸ BIPM defined the measured as the surface where the final value, where the measure is aimed (BIPM 2008)

⁹ The coverage factor defines the confidence interval of the measurement (Ball 2014).

A confidence interval of 95% is generally applied for the uncertainty measurement, and therefore, it is used a $k = 2$ (Luhmann et al. 2014; Stadek 2015; Barbero, Ureta 2011).

Uncertainty can be introduced in the measurement through external conditions and by the tester, the test procedure and many other factors that leads to wrong analysis or assumptions regarding the measurement (Ball 2014). Thus, during the measurement uncertainty calculation, the user must account for different sources of uncertainty associated to the measured object and measurement. The evaluation can be done either following an ISO standard or following the Guide to the expression of uncertainty in measurement (GUM).

GUM establishes general rules to account for different types of uncertainty (Ball 2014; JCGM 2008). The different uncertainty components influencing on the measurement are partitioned by GUM into two types, Type A and Type B. Type A accounts for observations acquired by repetition on the measurement and are statistically modelled. Type B, consider other sources of uncertainty where no repeatability is performed (Ball 2014; JCGM 2008).

The end result is given as Formula 2 and Formula 3, where both types of uncertainty can be joined through the combination of uncertainties. The combined uncertainty can be acquired through the following formula, which is also acknowledged as „root-sum-square“ (Ball 2014, p. 20):

$$u_c = \sqrt{\sum_i c_i^2 u_i^2} \quad (4)$$

According to Ball (2014) and (JCGM 2008), c_i^2 is defined as the sensitivity coefficient and u_i^2 is the standard uncertainty. For more information on how to calculate sensitivity coefficient the reader is advised to check the GUM guide and the work from Ball (2014).

To combine Type A and Type B on Formula 4, based on the work Ball (2014) drawn from the GUM, Type A and Type B must be accounted for their respective standard uncertainty. Type A evaluation is given by acquiring the mean and the standard deviation of the data (Ball 2014). While Type B is, according to the specifications of GUM, also treated according to its distribution. The analysis of which distribution to use must be made according to which knowledge and/or information the tester have on the evaluated uncertainty (JCGM 2008). When only the extreme values or no knowledge about the distribution is known, it is recommended the use of the rectangular distribution as defined in GUM guide (Ball 2014; JCGM 2008). Thus, type B standard uncertainty can be acquired through the following formula:

$$u_R = \frac{a}{\sqrt{3}} \quad (5)$$

Where, a is given by $\pm a$ which indicates the range of the data (Ball 2014).

To have the results as expanded uncertainty, as indicated by Formula 3 the coverage factor (k), must be indicated. According to Ball (2014, p. 21), „The coverage factor is a function of the effective

degrees of freedom for the combined uncertainty.” Thus, the used coverage factor to represent U defined according to each type of uncertainty is predominant over all standard uncertainties (Ball 2014). For more information on how to calculate k , the reader is advised to check the GUM guide and the work from Ball (2014).

In other to keep this section simple, only an indication of how to account for the measurement uncertainty was detailed. However, different factors of uncertainties leads to different evaluations. A good description of how to consider measurement uncertainty drawn from the GUM guide is available on the Ball (2014) work. Thus, it is highly recommended to check both works, the GUM guide and Ball (2014) for a better understanding.

2.2.3 Test Procedure Uncertainty

The VDI/VDE 2634 Part 2 and 3 covers the uncertainty regarding the test procedure, in other words, the uncertainty associated with the artefact and external conditions. Other sources of uncertainty as the measurement uncertainty associated with the system should be acquired by other means (VDI/VDE 2634 Part 2 2012).

The below uncertainties are used to assess the values acquired by the quality parameter. Thus, formula (6) and (7) and replaced in formula (1) to when checking for its compliance.

For the quality parameter *Probing Error*, the standard uncertainty defined by the guideline is:

$$u(p) = \sqrt{\left(\frac{F}{2}\right)^2 + u^2(F)} \quad (6)$$

where, F is the form deviation and $u(F)$ is the standard uncertainty of F (VDI/VDE 2634 Part 2; DIN ISO/TS 23165:2008-08).

In case other parameters influence the test procedure, as vibrations and instability of the mounted artefact, the test taker should also consider its influence in the calculation of the uncertainty. (VDI/VDE 2634 Part 2 2012).

For the quality parameter *Sphere Spacing Error (SD)*, the standard uncertainty defined by the guideline is:

$$u(SD) = \sqrt{u^2(\varepsilon_{cal}) + u^2(\varepsilon_{\alpha}) + u^2(\varepsilon_t) + u^2(\varepsilon_{fixt})} \quad (7)$$

where, $u^2(\varepsilon_{cal})$ standard uncertainty of the calibrated artifact; $u^2(\varepsilon_{\alpha})$ standard uncertainty of the linear thermal expansion of the artefact; $u^2(\varepsilon_t)$ standard uncertainty of the temperature; $u^2(\varepsilon_{fixt})$ standard uncertainty of the arrangement and installation of the artefact (VDI/VDE 2634 Part 2; DIN ISO/TS 23165:2008-08).

As for the quality parameter probing error, in case other parameters influence the uncertainty, it should be also included in the $u(SD)$ equation (VDI/VDE 2634 Part 2 2012).

For the quality parameter *Length Measurement Error (E)*, the same uncertainty equation will be used (VDI/VDE 2634 Part 3 2008).

At the end, the above standard uncertainties u must be given as expanded uncertainty U (VDI/VDE 2634 Part 2 2012), as indicated by Formula (3).

2.3 VISUALIZATION OF MEASUREMENT UNCERTAINTY

Visualization is a powerful tool that allows a better understand of the information being represented. With the amount of techniques available for data visualization, previous knowledge and a great understanding over the data is crucial. As data are not free of errors, the main difficulty arises in understanding and modelling uncertainty together with the data. When this task is performed effectively, the audience can reach another dimension of data perception. Thus, the awareness of the importance of uncertainty in visualization has expanded to other areas outside the academic and research level (Bonneau et al. 2014; Brodlie et al. 2012; Zhang et al. 2017, 2017).

Uncertainty is always a sensitive topic in data visualization. Most people handling data does not add the uncertainty at their visualizations, and therefore, report inconsistent and misleading information. Uncertainty is present in every data source. Uncertainty can be inherent from data acquisition or processing and modelling of the data, as well as, arising from both stages (Brodlie et al. 2012; Zhang et al. 2017; Pang et al. 1996). Therefore, representation should not display data as an accurate result. It must indicate the uncertainty level present in the observation (Bonneau et al. 2014; Brodlie et al. 2012; Sanyal et al. 2009; Pöthkow, Hege 2011; Grigoryan, Rheingans 2004; Pöthkow, Hege 2011)

According to Brodlie et al. (2012, p. 03), when the uncertainty is introduced during the acquisition stage it is designated as „visualization of uncertainty“. Moreover, when uncertainty arises from processing and modelling stage, it is named as „uncertainty of visualization“.

Uncertainty is therefore, one of the core parts of this master thesis. Following the general solution, the visualization of the measurement uncertainty will be employed in order to, aid the final user to enrich their knowledge over different geometric 3D acquisition methods.

In the next sub-section, a related work of visualization of uncertainty associated to measurand or generated data, is presented. The papers illustrated were crucial to establish a trajectory of what has already been done and assist in the preparation of the results in this thesis.

2.3.1 Related Work

Several works have been published containing uncertainty methods, modifications and applications. They provide an overview of techniques, introducing concepts and methods of how to consider the uncertainty in visualization. Brodlie et al. (2012) summed-up some difficulties in assigning uncertainty in visualization and listed some state-of-the-art techniques to represent uncertainty carried from the data acquisition or the processing stage. Likewise, Bonneau et al. (2014) address uncertainty

and methods for its evaluation and also provided an overview of various advanced approaches for visualizing uncertainty.

According to Bonneau et al. (2014), the evaluation of the uncertainty in visualization can be performed through: theoretical evaluation, low-level visual evaluation and task-oriented user study. With the task-oriented user study prevailing nowadays, over the others. An example is the work performed by Sanyal et al. (2009) where the authors performed a user test to evaluate and test the efficiency of common uncertainty techniques used in 1D and 2D representation. Another user study is proposed by van der Laan et al. (2015), where the authors evaluated the efficacy of 1D charts to represent uncertainty.

When dealing with statistical data and absolute length information, van der Laan et al. (2015) proposed the use of bar and line chart to represent uncertainty. Thus, in their work five different line charts and three bar charts, were analyzed. Through their online survey, participants were requested to analyze pattern in the data and evaluate the values depicted for the line chart and bar chart, respectively. The result was conditional to the value of the uncertainty range being represented. Thus for the line chart, ribbon associated with the line and error bars proved to be better. While for bar charts, error bars connected to bar charts and cigarette charts¹⁰ were preferred.

Another tool to represent uncertainty in data is using embed graph (Brodlie et al. 2012). In their user test, Sanyal et al. (2009) compared the efficiency of scaled and color glyphs, color mapping and error-bars. According to what was requested in the user test, each technique, except the error-bars, have excelled over the others. Pang et al. (1996) described glyphs as a very versatile tool for displaying uncertainty. Glyphs can be adjusted for different applications as to indicate flows and establish comparisons. Schmidt et al. (2004) used glyphs to represent uncertainty in multi-variate data. Their study analyzed glyphs in a lower dimension beforehand, where then the most representative was used in a higher level. The final glyphs were associated with additional features as color, touch and text, providing to the user the necessary amount of information to understand the uncertainty represented.

Brodlie et al. (2012) briefly mentioned that when uncertainty is associated with the data, a good approach to establish an analogy is by means of a best-fit model, if the geometry of the data is known. For the uncertainty analysis in their evaluation of different ranging sensors, Guidi et al. (2010) used the theoretical surface to compare the dispersion of each z coordinate. The authors computed the distance from the range map, extracted from the ranging sensor, to the best-fit plane to illustrate the dispersion. Barbero, Ureta (2011) also evaluated the dispersion of the point cloud based on the best-fit sphere generated. The authors used the normal distance from the points to the best-fit to visualize the dispersion in the data. To improve the visualization, the point cloud was clustered based on calculated distance using percentage values.

¹⁰ The cigarette chart introduced on the work of van der Laan et al. 2015, p. 04) allows the length representation in horizontal representation. The plot illustrates both extremes of the interval and does not require the representation of the point estimation.

Another similar approach is indicated by Grigoryan, Rheingans (2004) in their tumor growing application. Their approach made use of a local analysis, considering only one point at a time. The points were then, superimposed on a polygon surface, allowing the user to investigate the uncertainty based on the dispersion of the points.

Another efficient method for visualizing uncertainty is using a colormap. In Pöthkow, Hege (2011) evaluation and representation methods for uncertainty in isosurfaces and isolines, transparency and color were used to represent crispy surfaces. The uncertainty used in their visualization assumed measurement and computation error as one.

Representing uncertainty is a growing field and many applications were mentioned above. Still, as noticed by Pang et al. (1996) and Sanyal et al. (2009), it is crucial to understand the data before applying any technique to it. Schmidt et al. (2004) at the end of their work, listed a guideline of how to represent uncertainty in several dimensions. The authors pointed that uncertainty will rely heavily on which information/feature the user wants to highlight. According to Pang et al. (1996) uncertainty should support decision making and thus, its representation should restrain to visualizations that can benefit from it.

This master thesis slightly varies from most of the work above specified, since here the emphasis is given to the uncertainty. As mentioned previously, visualization is being add to support the general solution and reduce the complexity of the discussed theme. Hence, in this research uncertainty is foremost than the data representation.

3 STUDY CASE

3.1 Cultural Heritage Digitization (CHD)

The Competence Center Cultural Heritage Digitization department at Fraunhofer IGD - Darmstadt, has developed over the years scanning technologies in order to improve their work with 3D digitization of cultural heritage objects.

The equipment that will be evaluated based on the research solution are prototypes or integrate solutions of digitization systems developed by the CHD department. Thus, the study case of this research is composed of Nikon D610 with AF-S Nikkor 50mm lens, Canon 5DSr with Canon 100mm lens and a laser line scanner.

3.1.1 Equipment characteristics

3.1.1.1 Photogrammetric systems

As mentioned in 2.1.2.1, camera settings can influence considerably in the measurement. Therefore, a special attention should be given when choosing the appropriate settings for the image acquisition. The settings used in the daily activities of the department and thus, in this research were retrieved based on the DxOMark Image Lens evaluations.

DxOMark evaluates settings of cameras and lens to provide measurements rating. Their work consists of testing cameras and lenses under systematic conditions, providing an extended database where user can find the measurement and appropriate settings for each camera + lens combinations (DxOMark 2017).

Table 1 and Table 2 provide an overview of the settings used for the Canon 5DSr with Canon 100mm lens and Nikon D610 with AF-S Nikkor 50mm lens, respectively.

Table 1: Canon 5DSr + Canon 100mm lens settings overview

Canon 5DSr + Sigma 100mm lens	
Aperture	f/16
ISO	200
Exposure time	1/50
Sensor – object distance	45 cm

Table 2: Nikon D610 + AF-S Nikkor 50mm lens settings overview

Nikon D610 + AF-S Nikkor 50mm lens	
Aperture	f/14
ISO	200
Exposure time	1/50
Sensor – object distance	47 cm

Before the acquisition of each adapted test, the calibration of the system under test was performed. For the system calibration, a plate with coded targets and features was used.

In this master thesis, during the evaluation of the sensors Nikon D610 + AF-S Nikkor 50mm lens will be referred as photogrammetric system I and Canon 5DSr + Canon 100mm lens as photogrammetric system II.

3.1.2 Laser Line System

As mentioned above, the laser line evaluated in this research is a prototype developed by the CHD department. Hence, the operational characteristic of the sensor differ from available laser line scanners in the market. For a better comprehension of the scanning system, a brief description provided by the department is presented below.

➤ Laser Line sensor

The system consists of two main components. The first is the sensor itself which is based on the principal of laser line triangulation and the second is a robot arm which can move the sensor around the object.

To acquire a 3D model the system will automatically move the sensor around the object using the robot arm. The sensor can then locate the laser line in the camera image and estimate the 3D position of every line point. Because this 3D position is still in sensor coordinates it has to be transformed to world coordinates by using the information from the mechanical system (Blais 2004).

As a prerequisite the system has to be calibrated, which is done in multiple steps. The robot arm itself is calibrated by the manufacturer. The sensor calibration is performed with the aid of a calibrated board. For each position of the sensor, one set of images is taken by illuminating the entire board and the other by projecting the laser line on it. Likewise the photogrammetric approach specified above, the camera calibration follows the same method. After the camera calibration is finished it is possible to extract the depth value for every detected line location because the geometry of the calibration target is known. A plane is then fitted to this set of points to calibrate the laser plane. As a result it is possible to estimate the depth for objects with unknown objects, just by locating the line in the camera image.

The entire reconstruction is achieved by referencing all positions to a common coordinate system, through the mechanical coordinates from the robot arm.

3.1.3 Sensor Measuring Volume and Measurement Volume

Following the description given on □ of this research, the quality parameters are acquired by measuring calibrated objects. The objects are manufactured based on the spatial diagonal of the sensor measuring volume and body diagonal of the measurement volume.

The sensor measuring volume of an image is defined as the volume measured in a single image (VDI/VDE 2634 Part 3 2008), and it is specified by the sensor of the scanning system. While,

measurement volume is defined by the set of images that defines the volume of the measured object (VDI/VDE 2634 Part 3 2008). In other words, measurement volume defines theoretically the limiting area for the scan system (Mendricky 2016; SMARTTECH 3D scanners n.d). More information on how these values are defined can be found in the Appendix part of this research (see A).

These concepts are specific for each sensor. For photogrammetric systems, the values can also change according to the settings being used. Therefore, when evaluating optical 3D scanning systems the manufacture must state measurement and sensor measurement volume.

Measurement and sensor measurement volume for the evaluated equipment used in this master thesis, is indicated in Table 3 and Table 4.

Table 3: Sensor measuring volume of the evaluated scanning systems

Sensor Measuring Volume					
Scan System	Angle of View			Depth-of-field	
	Horizontal	Vertical	Diagonal	Near plane [mm]	Far plane [mm]
Laser line scanner	20.0	10.0	22.3	350	450
Nikon D610 + AF-S Nikkor 50mm lens	39.6	27.0	46.8	442	502
Canon 5DSr + Canon 100mm lens	20.4	13.7	24.4	443	458

Table 4: Measurement volume of the evaluated scan systems

Scanning System	Measurement Volume [mm]
Laser Line Scanner	500 x 500 x 500
Nikon D610 + AF-S Nikkor 50mm lens	420 x 420 x 600
Canon 5DSr + Canon 100mm lens	200 x 200 x 300

3.1.4 Experiment setup

The setup for the photogrammetric systems consisted of:

- The evaluated camera + lens combination;
- The artefact in accordance with the evaluated sensor;
- Four flashes;
- One umbrella;
- Two softboxes;
- One CamRanger, to automatically acquire the images;

- One turntable.

The setup for the laser line scanner system consisted of:

- The laser line sensor;
- One robot arm, to define the trajectory;
- The artefact in accordance with the evaluated sensor.

4 METHODOLOGY

4.1 WORKFLOW

This chapter provides a detailed description of the work carried out in this master thesis. To generate our general solution and address the research objectives, the problem statement was divided in different phases, as indicated in Figure 10.

The first phase comprehend the input preparation. Thus, this part will cover the artefact design and preparation. The proposed tests for assessing the accuracy and point cloud acquisition is detailed on the second phase. The best-fit algorithm used to extract the theoretical surface as well as the evaluation of each quality parameter is detailed in phase three. The fourth phase includes uncertainty analysis. The assumptions drawn to visualize the measurement uncertainty and a description of the online survey performed is described here.

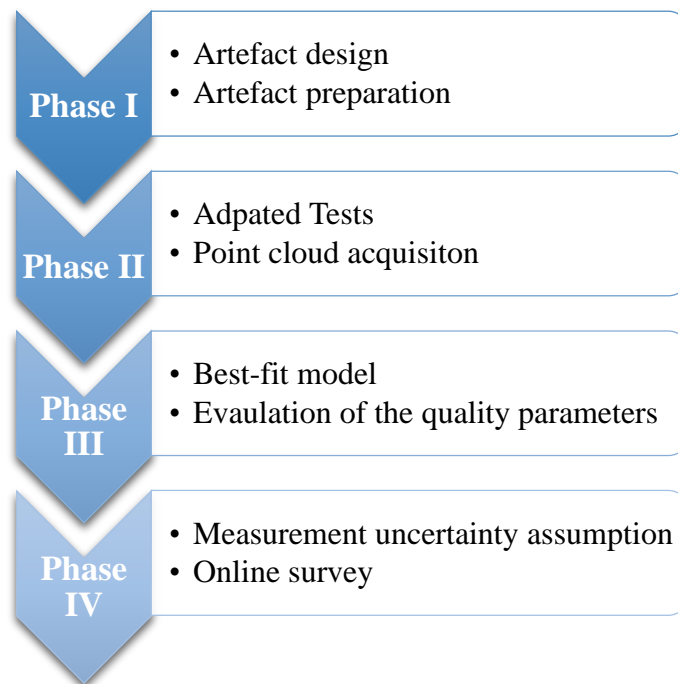


Figure 10: Methodology overview

4.2 INPUT PREPARATION

4.2.1 Artefact design

To evaluate the accuracy of optical 3D scanning systems of calibrated objects, termed in this research and in the VDI/VDE 2634 Part 3 is defined as artefacts, are necessary. Thus, specially designed artefacts were manufactured for the application of the proposed solution.

The artefact used during the test is in accordance to the specifications of the guideline. Thus, sphere plates were designed to comply with the guideline requirements. The sphere plates consist of two

spheres mounted on a plate. The spheres dimensions are in accordance with the sensor measuring volume and the plate length is tested with the measurement volume of each scan systems. Figure 11 provides an illustration of the spheres and plates, for more information of sensor and measuring volume please refer to Table 3 and Table 4

The spheres were manufactured and calibrated according to the DIN 5401 standard. They are also extra polished, agreeing with the artefact properties established by the VDI/VDE 2634. The spheres were bought from Kugel-Winnie in Germany. Table 5 presents more information of each sphere manufactured for this research. The plate specially designed for this master thesis, fits each sphere with high precision. The spheres are fitted on the plate through calibrated holes, located in each extreme of it. The plate was manufacture by the Werkstatt für Feinmechanik at TU Darmstadt, who also ensure its accuracy. Table 6 presents the length, used as ground truth during the comparison with the measured one, and its associated standard uncertainty.

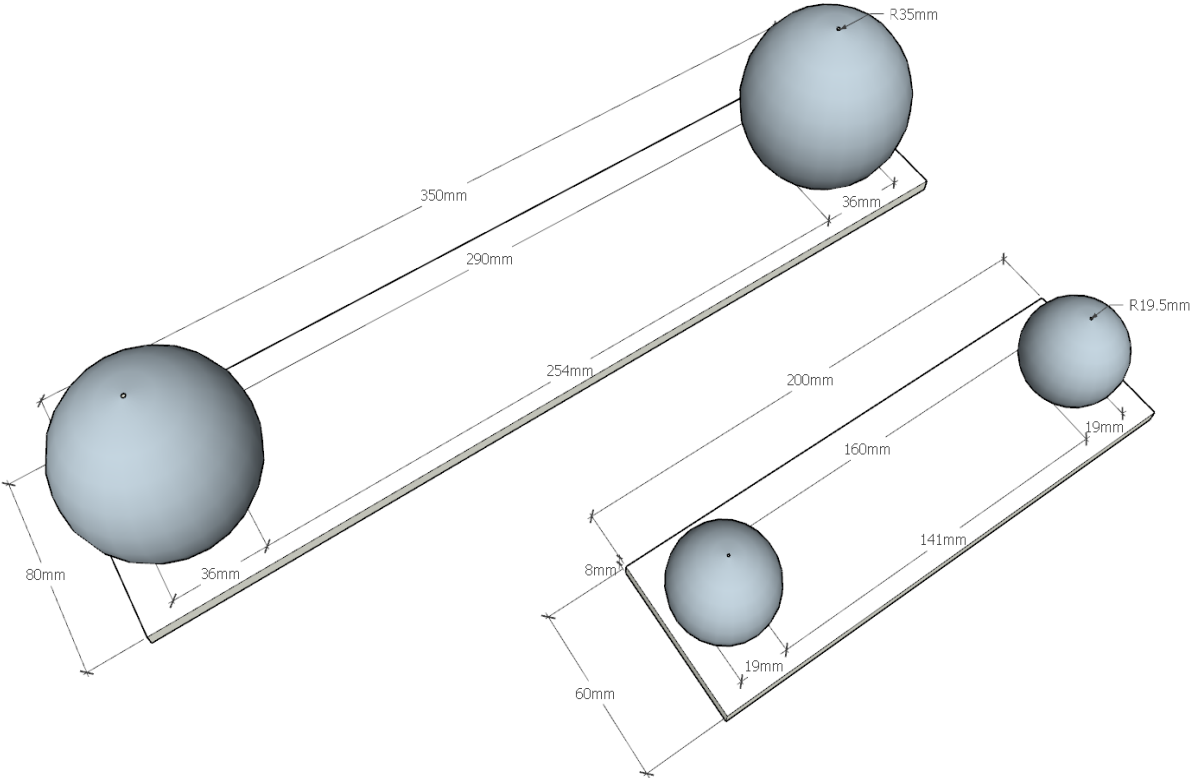


Figure 11: Sketch of the spheres plates created in SketchUp

Table 5: Sphere specifications according to the DIN 5401 (RGPBALLS 2017)

Sphere specifications		
Quality	Nominal diameter (mm)	Standard uncertainty (μm)
G28	38	± 13.7
G40	70	± 19.0

Table 6: Plate specifications according to the specifications of the manufacturer

Plate specifications	
Nominal length ¹¹ (mm)	Standard uncertainty (μm)
160	± 10.0
290	± 10.0

4.2.2 Artefact preparation

As the spheres were manufactured with chrome steel material, its reflective surface does not allow the reconstruction and therefore void the triangulation system principle (Beraldin et al. 2012). According to Robson et al. (2011, p. 4), the spheres must have a „cooperative surface“. The reflection should approximate to a Lambertian reflection, which indicates an ideal reflection, and the properties of the spheres should have minimal influence on the measurement being made (Beraldin et al. 2015; Carmignato, Savio 2011; Robson et al. 2011).

Therefore, surface treatment places a great importance when testing scanning systems. According to Robson et al. (2011, p. 4), surface treatments like „vapour blasting, light particle or spray particle coating“ can be used to acquire the desired effect. However, the user must be aware that the coating applied can exert great influence on the measurement being made, as coating are sometimes not even. An example of coating effect and its deviations is illustrated in the work of Mendricky (2016). As pointed by Beraldin et al. (2015), when coating is used to treat the sphere, the calibration is voided.

In this research an automotive painting was used for surface treatment. Different types of coatings compose the automotive painting and from these, the basecoat generally presents minimal thickness. Thus, to treat the glossiness of the spheres a black matte basecoat was used.

With a relatively small thickness being added on the spheres, tests can be performed to prove that no additional layer will influence in the measurement and therefore, not voiding the artefact calibration. The test consists of adding the matte basecoat to a reference object, with a distinguish number of layers on defined areas. The plate is then, checked for bumps occurrence by comparing the different numbers of coating sprayed. Objects with known geometric shapes can be used to reproduce the test, in this master thesis a metal plate was used.

The test procedure was performed as follows. First, two layers of coating were sprayed on the plate. After drying, the middle part was covered and three additional layers were sprayed on the top part and five additional layers on the bottom of the plate. Figure 12 illustrates the plate used for the test, as well as an indication for the number of layers.

¹¹ The length indicated in the table refers to the length in between the spheres centers. As mentioned in Chapter 3, these lengths are measured with the evaluated scans for the assessment of the SD error.

For the acquisition stage, an equipment of higher resolution should be used. In this master thesis a macro-lens camera (Canon 5DSr + Canon100mm lens) was used. Once measurements made with it can detect more features and thus, being more precise. Following the rules of photogrammetry briefly



Figure 12: Coating indication

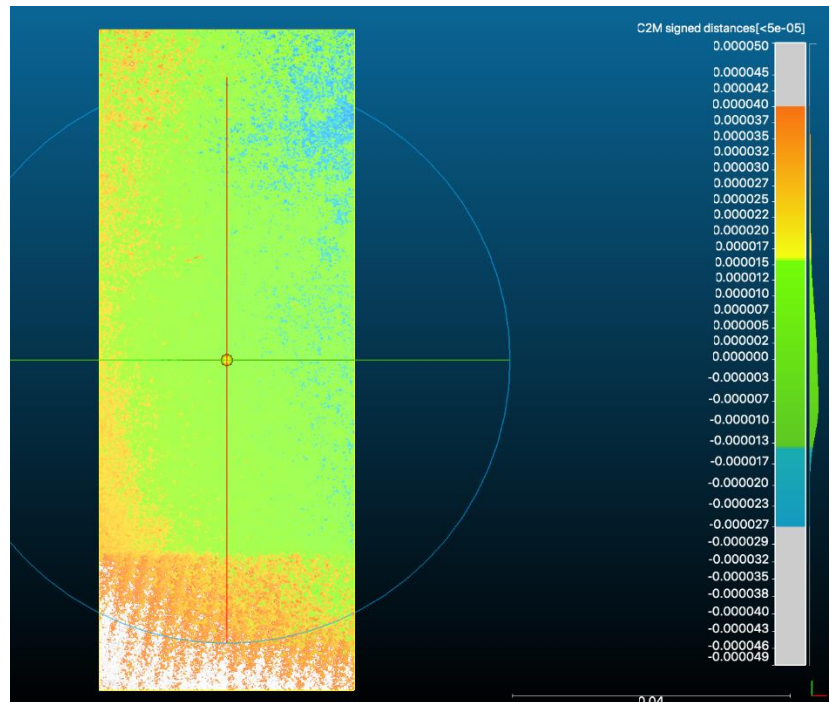


Figure 13: Coating evaluation performed in CloudCompare

explained in 0, good overlapping area should be ensured during the acquisition. Thus, the sensor was positioned in two heights and 192 images were captured.

The test evaluation was done by fitting a best-fit plane on the area having two layers of coating. The fitted plane worked as the ground truth during the evaluation of top and bottom part of the plate. Bumps occurrence was evaluated using a signed distance function¹². Software that can perform signed distance function or simply compare height difference can be used to replicate this test. In this master thesis, the test was performed with the software package CloudCompare.

As expected, the result indicates that no bumps were detected between the top and middle part of the plate, the five and two layers coating respectively. The signed distance accounted a variation of $\pm 15\mu m$ ¹³ and this value will be incorporated to the standard uncertainty of the calibrated object (ϵ_{cal}), indicated in Formula 7. Figure 13 illustrates the results encountered on the test.

After confirming that the layers would not affect the measurements, the matte basecoat was used on the spheres. As the coating application can vary from operator to operator, one single person should

¹² The signed distance function works by comparing the distance from the point cloud to the ground truth, represented as a mesh. [CloudCompare - Cloud-to-Mesh Distance](#), Accessed December 2nd, 2017.

¹³ In CloudCompare the units derive from the point cloud, [CloudCompare - Forum](#). Accessed December 2nd, 2017.

be in charge of performing it. To achieve a homogeneous application, a string suspended the spheres and its rotation was induced.

The coated spheres could then be mounted on the plate. To support the registration and scale of the artefact on photogrammetric evaluation, coded markers and additional features can be placed on top of the spheres-plate. Figure 13 illustrates the small sphere-plate used in this master thesis before and after its preparation.



Figure 14: Sphere plate before and after its preparation

4.3 Adapted tests

Replicating the test according to specifications of the VDI/VDE 2634 (see Chapter 3), proved to be impractical when following the photogrammetric rules. Thus, some modifications in the procedure of acquiring the images were performed to better agree with photogrammetry principles. As this master thesis aims to establish a common approach for all scan systems evaluated here, all tests were performed following the same approach, as described in the next sub-sections.

The adapted tests were performed in laboratory with controlled conditions, as temperature, illumination and had no influence of external light. For acclimatization, the evaluated scan system and artefacts were placed in the laboratory 12 hours before the measurement acquisition.

4.3.1 Probing Error test

For the joint acquisition of the Probing Error, only one position was successfully defined within the measurement volume. Therefore, to still comply with the description in the guideline the sphere was evaluated by placing the sensor in three arbitrary heights. For each height, the sphere was lying in different positions inside the sensor measuring volume. By modifying the position within the sensor measuring volume, the quality parameter tests the ability of the scan to register images/point cloud when non-optimal positions are adopted.

The system setup is defined for each evaluated scan system, as specified in 3.1.4. The measurement was performed in a vibration free environment, the illumination considered only artificial source of light and the temperature in the laboratory was checked in intervals of 30 min. The temperature variations were accounted for the evaluated scan system and artefact.

For the assessment of the image/point cloud for the Probing Error parameter, only one sphere of the sphere-plate is necessary. Each height acquisition, corresponds to 32 images/lines taken from a 360° rotation. Thus, three datasets for each evaluated optical 3D scan system were acquired at the end.

For the photogrammetric approach, coded targets placed on top of the sphere-plate referenced the sphere coordinates to a local coordinate system.

4.3.2 Sphere Spacing Error test

For the acquisition of the SD quality parameter, from the seven positions suggested in the guideline (see Figure 9) only three positions could be successfully defined.

As well as for the Probing Error acquisition, each setup was mounted with the tools and equipment described in section 3.1.4. The measurements were performed under the same conditions as described in the Probing Error test.

For the assessment of the image/point cloud for the SD quality parameter, the sphere-plate was positioned on 0°, 45° and 90° within the measurement volume (Figure 15). These angles represent each adopted position to evaluate the sensors.

For each position, the sensor was placed in two arbitrary heights and the acquisition of images/point cloud was performed focusing one sphere at a time. For each sphere, 64 images/lines were acquired from a 360° rotation. Thus, each dataset corresponds to 128 images/lines.

For the photogrammetric approach, images were captured in between when translating the focus from one to another. The procedure is employed to support the registration and reference the sphere to a common coordinate system.



Figure 15: Defined positions for the SD acquisition

4.3.3 Length Measurement Error test

The E quality parameter is evaluated according to Method A described in the guideline. The Method takes the results acquired for the Probing Error and Sphere Spacing Error into consideration and thus, the evaluation considers the worst case scenario.

According to the VDI/VDE 2634 Part 3, due to averaging effects when registering the acquired images/line the PF is not fully inserted in the SD evaluation. Thus, to define the overall error of the length, E must be introduced on the evaluation of the sensor under test (VDI/VDE 2634 Part 3 2008).

E evaluation does not require any additional test and thus, the results will be presented in Chapter 5.

4.4 Point cloud acquisition

It is important to mention that several sources of errors are introduced on the measurement during the reconstruction. Therefore, the user must be aware of this when choosing the reconstruction algorithm (Sims-Waterhouse et al. 2017).

In this master thesis, the reconstruction of the point cloud was performed with the software package Agisoft PhotoScan. To ensure higher trust, the process used normal calibration, as defined in 0. After the acquisition of the intrinsic parameters the alignment was performed. Agisoft PhotoScan uses feature detection and SfM to align photos as indicated on 0. The point cloud is reconstructed at the end of the alignment. The final output point cloud should contain only the measured objects. In other words, the point cloud should contain only the spheres.

No refinement or filtering is performed during this stage. As mentioned in 2.1.4, the guideline does not recommend the use of filtering, unless they belong to the normal modes of operation.

For the laser line sensor, the reconstruction occurs in real time. Due to the trajectory defined by the robot arm, the lines are already registered and the point cloud is acquired with the end of the measurement. For further information, please revise 0 of this master thesis.

4.5 Best-fit algorithm

Following the specification of the guideline, for the evaluation of the quality parameters a least-squares method with variable radius should be applied (VDI/VDE 2634 Part 3 2008). Thus, a best-fit model based on Gaussian-Newton method was developed with the Matlab software package. A good description about the related method can be found in Forbes (1989) technical paper and in Panyam (2007) master thesis.

The input file used on for the best-fit algorithm is derived from the point cloud acquired in the previous step. The 3D coordinates of each sphere should be separately converted to a .csv file.

4.5.1 Assumption

For a good performance of the algorithm, some considerations should be made.

As pointed by Forbes (1989), to retrieve accurate results from the best-fit algorithm based on the Gaussian-Newton method, the data must be representative;

As least squares methods are used to minimize the sum, tolerance criteria should be provided for the algorithm convergence (Forbes 1989; Panyam 2007). Thus, a tolerance of 10^{-6} was applied. The tolerance can be justified, the metric units adopted is meters and any value below the defined tolerance are not relevant.

4.5.2 Algorithm Framework

The algorithm framework is partitioned in three steps, as illustrated by Figure 16.

The best-fit sphere algorithm requires an initial estimate, before minimizing the sum (Forbes 1989). Thus, the first step of the algorithm is entitled to calculate the estimate. According to the (VDI/VDE 2634 Part 3 2008), three out of one thousand points can be removed from the data. Thus, the second step is responsible for removing the outliers of the input data. The third step is used to minimize the sum and return the best-fit sphere.

Although all steps belong to the best-fit sphere algorithm, they will be explained separately in the next sub-sections. The algorithm created in Matlab is also available in the Appendix part of this research (see B).



Figure 16: Best-fit algorithm steps

4.5.3 Sphere Fit

To acquire the initial estimate, the following procedure was applied. As defined by Forbes (1989), the initial estimate constitute of the minimization of distance between the point cloud and the sphere. Thus, the problem can be defined as follows. The procedure is explained by Forbes (1989), Sims-Waterhouse et al. (2017) and Jekel (2015).

The input value used in this function is the 3D coordinate of the evaluated point cloud.

As the geometry being fitted corresponding to a sphere, the evaluation will based on the sphere equation. Thus, the equation:

$$r_i^2 = (xi - a)^2 + (yi - b)^2 + (zi - c)^2 \quad (8)$$

where xi , yi and zi are the initial coordinates, $x0$, $y0$ and $z0$ are the center of the sphere and r is the radius (Forbes 1989; Jekel 2015; Sims-Waterhouse et al. 2017).

When expanding and rearranging the terms of Formula 08, the problem can by solved simply as a linear equation. Thus, Formula 08, become:

$$A \cdot X = B \quad (9)$$

Where X is vector, defined as:

$$X = \begin{bmatrix} a \\ b \\ c \\ D \end{bmatrix} \quad (10)$$

where a , b and c are the initial estimative of the center of the sphere and D corresponds to the diameter of the sphere (Forbes 1989; Jekel 2015; Sims-Waterhouse et al. 2017).

The estimate radius is then, given by the following formula (Forbes 1989; Jekel 2015; Sims-Waterhouse et al. 2017):

$$r = \sqrt{a^2 + b^2 + c^2 - D} \quad (11)$$

The above steps constitute then, the initial estimation for the center of the sphere and the radius.

This part of the algorithm was created as a Matlab function and is available on the Appendix part of this paper (see Ba).

4.5.4 Radial error

The second step of the algorithm named as radial error was developed to comply with the specification of the VDI/VDE 2634 Part 3. The input of this function is composed by the 3D coordinate of the evaluated point cloud, the estimate radius and center of the spheres.

By using the values acquired in the previous step, the radial error is calculated. This formula encompass the distance from each 3D coordinate to the initial best-fit sphere estimation, given by initial estimate of the center and the radius. Thus, the radial error can be defined as:

$$\Delta r = r_i^2 - r^2 \quad (12)$$

where r_i is given by Formula 08 and r is the initial estimative of the radius (Sims-Waterhouse et al. 2017).

Formula 09 gives the dispersion of the point cloud. Thus, based on the radial error vector the outliers will be removed.

To remove the 0.003% allowed by the guideline, the radial error vector was used to identify the outliers position. Thus, radial error vector was partitioned as $\Delta r > 99.97\%$ and $\Delta r \leq 99.97\%$. As the dispersion values can be negative or positive, when defining the threshold the absolute value should be considered. Thus, above explanation can be translated Matlab as:

$$threshold = quantile(abs(\Delta r), 0.997) \quad (13)$$

After identifying and removing the outliers in the radial error vector, a loop was performed to locate relative position of these values in the 3D coordinate matrix. After its identification, the outliers were removed from the 3D coordinate matrix.

The output of this function is then the updated 3D coordinate matrix. This part of the algorithm was created as a Matlab function and is available on the Appendix part of this research (see Bb).

4.5.5 Minimization

The last function that composes the algorithm, use the Gaussian-Newton method to minimize the sum and provide the final estimation for the center and radius of the sphere.

The input of this function is the updated 3D coordinate acquired from the *Radial Error function*. Due to the outliers removal, the new matrix entries is smaller by the same amount of outliers that were removed. Thus, in order to update the center and radius of the sphere for the new matrix, the *Sphere Fit* function should be evaluated again.

With all updated values, Formula 12, is calculated again. At this point, all values in the function were updated for the new 3D coordinate matrix.

With the all values updated, the Jacobian¹⁴ matrix for Δr is calculated (Forbes 1989). The employed calculation is given by:

$$J = \begin{bmatrix} \frac{\partial(\Delta r_i)}{\partial a} & \frac{\partial(\Delta r_i)}{\partial b} & \frac{\partial(\Delta r_i)}{\partial c} & \frac{\partial(\Delta r_i)}{\partial r} \\ \vdots & & \ddots & \vdots \\ \frac{\partial(\Delta r_m)}{\partial a} & \frac{\partial(\Delta r_m)}{\partial b} & \frac{\partial(\Delta r_m)}{\partial c} & \frac{\partial(\Delta r_m)}{\partial r} \end{bmatrix} \quad (14)$$

where $\Delta r_i \dots \Delta r_m$ indicates all entries of the radial error vector; a , b , c are the center of the spheres and r the radius of the spheres (Forbes 1989).

After acquiring the Jacobian matrix, the function finds the residuals by solving another linear equation (Forbes 1989). Therefore:

$$J^T \cdot J \cdot v = J^T \cdot (-\Delta r) \quad (15)$$

where, J^T is the transposed matrix of the Jacobian (J); v is the residulas and Δr is radial error, defined in Formula 12 (Forbes 1989).

After acquiring the residuals, the center and radius of the spheres are incremented (Forbes 1989).

¹⁴ The Jacobian matrix derives a function, in this case Δr , based on a specific variable (Forbes 1989).

The entire process is incremented until the algorithm converges (Forbes 1989). The convergence is reached when the absolute sum of the residuals is smaller than the tolerance, which in this master thesis is assumed to be 10^{-6} [m].

The output at the end is the best-fit sphere. Where the sphere center and radius is used to derive the quality parameters.

This part of the algorithm was created as a Matlab function and is available on the Appendix part of this research (see Bc).

4.6 Evaluation and assessment of the adapted tests

4.6.1 Assumption

The guideline recommends that the assessment has to be performed for all measured positions of each quality parameter. After the values being assessed, the final value is given by the greatest value among the measured positions in each quality parameter (Mendricky 2016). In this master thesis however, the final value for each quality parameter will be given as the mean value.

4.6.2 Evaluation of the adapted tests

The above algorithm constitutes the bases for the evaluation of each quality parameter. Thus, using the software package Matlab a *Script* was created to run the functions SphereFit, Radial Error and Minimization. The input for the evaluation of each quality parameter arises from the results of the Best-fit algorithm.

Although the steps are being explained separately, the Script was create to calculate dynamically a sequence of files. One Script was developed for joint acquisition of the Probing Error and one Script for the SD. For the execution of the Script, it is necessary to add on the same folder the .csv files, corresponding to the evaluated parameter, the Best-fit algorithm and the Script itself. The scripts generated in this part are available in the Appendix part of this master thesis (see Bd).

For the evaluation of the Length Measurement Error (E), a Matlab function was created once its analysis is dependent on the result of the Sphere Spacing Error (SD) and the Probing Error (PF and PS).

4.6.2.1 Probing error

After acquiring the results from the Best-fit algorithm, the Probing Error, Form and Size, was evaluated. As mentioned in 2.1.4.1, PF is defined as the range between the max and min radial deviation from the measured points to the theoretical surface, best-fit sphere. And the PS is given by the mean value of the measured diameter subtracted from the calibrated one (VDI/VDE 2634 Part 3 2008). To indicate the dispersion of the data. Thus, the calculation of each quality parameter is as follows.

4.6.2.1.1 Probing Error Form Evaluation

As mentioned in 2.1.4.1, PF indicates the ability of the sensor in measuring forms. Therefore, its results use the radial error, indicated by Formula 16. As described in the 0, PF test is performed in three arbitrary positions where for each position a PF value will be assigned.

PF is then, given by the following formula (Mendricky 2016; Sims-Waterhouse et al. 2017):

$$PF_{pos} = \sigma(\Delta r) \quad (16)$$

where, Δr is the radial error matrix generated in the Best-fit algorithm.

The ability of the sensor was then given as one result, by calculating the mean value from Formula 14 (Sims-Waterhouse et al. 2017) as:

$$PF = \frac{\sum \sigma(\Delta r)}{n} \quad (17)$$

with n indicating the number of measured positions.

4.6.2.1.2 Probing Error Size (PS) evaluation

As mentioned in 2.1.4.1, PS is defined by the guideline as the difference between the diameter from each calculated best-fit sphere to the calibrated diameter (VDI/VDE 2634 Part 3 2008). Thus, the calculation is as follows:

$$PS_{pos} = Dm_{PF} - D_{calib} \quad (18)$$

where, Dm indicates the measured diameter and D_{calib} as the calibrated diameter.

For the final value acquisition, the mean value was retrieved from Formula (18). As the result is given as a mean value, the standard deviation for the mean was also calculated in this step by (Sims-Waterhouse et al. 2017; JCGM 2008):

$$\sigma(mean) = \frac{\sigma(D)}{\sqrt{n}} \quad (19)$$

where, $\sigma(D)$ is the standard deviation of the measured diameters and n is the number of measured positions (JCGM 2008).

4.6.2.2 Sphere Spacing Error

For each measured position, the length in between the centers of spheres was calculated using an Euclidian distance. After acquiring the length for each measured position, the SD was acquired by subtracting the measured length from the calibrated length, as specified in the VDI/VDE 2634 Part 3. Thus, these steps can be calculated as:

$$Dist = \sqrt{(a1 - a2)^2 + (b1 - b2)^2 + (c1 - c2)^2} \quad (20)$$

where, $a1, b1, c1$ are the center of the first sphere and $a2, b2, c2$ are the center of the second sphere located in the sphere-plate.

$$SD_{pos} = Lm_{SD} - L_{calib} \quad (21)$$

where, Lm_{SD} indicates each measured length and L_{calib} the calibrated length (VDI/VDE 2634 Part 3 2008).

After the acquisition of the SD quality parameter the standard deviation of the mean was also calculated, as indicated in Formula (19) (Sims-Waterhouse et al. 2017). However, it is considered the SD_{pos} value instead of the diameter.

4.6.2.3 Length Measurement Error (E) evaluation

The Length Measurement Error (E) was evaluated according to its description in the guideline. Thus, for the calculation of this quality parameter, a *if loop* was generated to consider all covered possibilities from the Method A, as defined in the guideline. The input value for this function requires the PS, PF, distances acquired by each position in the evaluated position of the SD and the calibrated length.

Thus, the E can be given as (VDI/VDE 2634 Part 3 2008):

$$if (SD_{pos} + PS_{pos}) \begin{cases} > 0; E = (SD_{pos} + PS_{pos} + PF_{pos}) \\ = 0; E = PF_{pos} \\ < 0; E = (SD_{pos} + PS_{pos} - PF_{pos}) \end{cases} \quad (22)$$

where, SD_{pos} is given by Formula (21), PS_{pos} by Formula (18) and PF_{pos} by Formula (16).

4.6.3 Assessment test

The assessment test will be made individually for each measured position even though, in this thesis the mean value is used to represent each quality parameter. Thus, after acquiring the parameters in the evaluation test, the results were compared to MPE_{xx} relative to each scan system minus the U relative to the test procedure, according to Formula (1). If all the values are below this limit, the accuracy of the system is assessed and then, the mean value is used to represent it.

4.7 Measurement uncertainty evaluation

4.7.1 Assumption

For the evaluation of the measurement uncertainty (see 2.2.2), some assumptions must be made in order to simplify the calculations but, at the same time providing a good confidence interval from where the ground truth can be found.

The measurement uncertainty analyzed in this master thesis will refer to the uncertainty in the measurement and pre-processing stage, when the point cloud is acquired. Furthermore, this research will only treat uncorrelated data and will not consider systematic error. Which is reinforced by the GUM guide choice, where the standard does not account for any systematic error. The evaluation is regarded only to the uncertainty arising from it (Farrance, I., & Frenkel, R. 2012).

Thereby, this master thesis will analyze uncertainty in a similar way as Pöthkow, Hege (2011). The authors evaluated the entire process, measurement and processing stage, as a whole and did not evaluate the influence from systematic errors. Thus, this research will also not make distinction on the types of uncertainty accounted. The results will be based only on the measurement uncertainty, without specifying from where it was derived.

As indicated in 0, the measurement uncertainty in this master thesis will be evaluated by means of the GUM guide and the uncertainty evaluation suggested by the guideline. Thus, the below steps will indicate the evaluation procedure as well as the sources of uncertainty considered.

4.7.1.1 Test procedure uncertainty evaluation

According to the guideline, for the assessment of the quality parameters the uncertainty associated to the test procedure (see 2.2.3) should be acquired for each evaluated quality parameter (VDI/VDE 2634 Part 2 2012). Thus, their evaluation is detailed in the below sub-sections.

4.7.1.1.1 Probing Error uncertainty evaluation

The uncertainty associated to the Probing Error arises only from the calibration of the spheres. Thus, the evaluation simply resumes to Formula (6), where values for each parameter indicated can be found in the table below.

Table 7: Calibration values according to DIN 5401 (RGPBALLS 2017)

Probing Error – sphere calibration values			
G40 (70mm sphere)		G28 (38mm sphere)	
Form deviation - F	Standard uncertainty - $u(F)$	Form deviation - F	Standard uncertainty - $u(F)$
$1\mu m$	$\pm 19.0\mu m$	$0.7\mu m$	$\pm 13.7\mu m$

4.7.1.1.2 Sphere Spacing Error and Length Measurement Error uncertainty evaluation

The uncertainty considered for SD and E quality parameters can be acquired through Formula (7), where its values are calculated based on the DIN ISO/TS 23165:2008-08.

As described in the DIN ISO/TS 23165:2008-08, the standard uncertainties $u(\varepsilon_\alpha)$ and $u(\varepsilon_t)$ are only accounted if the sensor can be thermally compensated, in all other cases these values should be set to zero. In addition, the standard uncertainty $u(\varepsilon_{fixt})$ was also set to zero. This standard uncertainty refers to the fixture of the material during the measurement and once all recommendations were

follow, such assumption could be made. Thus, at the end only the standard uncertainty for the artefact, $u(\varepsilon_{cal})$, was considered.

As mentioned previously, for the calculation of $u(\varepsilon_{cal})$ besides the uncertainty of the sphere calibration, it is also necessary to account for uncertainty of the coating and plate. As three parameters are influencing on the same component, the quadratic mean uncertainty must be used to calculate them (Barbero, Ureta 2011). Thus the standard uncertainty for the artefact can be evaluated through:

$$u(\varepsilon_{cal}) = \sqrt{\frac{u^2_{sphere} + u^2_{coating} + u^2_{plate}}{3}} \quad (23)$$

where, u^2_{sphere} is given the standard uncertainty of the calibration artefact (see Table 7); $u^2_{coating}$ was acquired during the artefact preparation (see 4.2.2) and; the standard uncertainty of the plate is provided by the manufacturer (see Table 6).

4.7.1.2 Measurement uncertainty evaluation

Besides the uncertainties of the test procedure, the uncertainty associated to the final value will also account for the randomness in the measurement and for the inaccuracy when defining the local coordinate system during the point cloud acquisition/reconstruction.

The randomness in the measurement is acquired during the evaluation of the quality parameters. For the PF it is the mean of the standard deviations acquired for each measured positions, Formula (17), while for the others parameters the standard deviation of the mean, Formula (19), will be used. According to JCGM 2008, these uncertainties are calculated as uncertainty Type A (see 2.2.2).

The inaccuracy for the local coordinate system is dependent on the evaluated sensor. Thus, in the photogrammetric approach, this value derives from the displacement of the center of the target in relation to the local coordinate system. While, for the laser line arises from the mechanical coordinate of the robot. Both values were provided by CHD, the study case of this research. According to JCGM 2008, these uncertainties are calculated as uncertainty Type B (see 2.2.2).

Thus, the calculation of the measurement uncertainty will then follow the GUM guide adding all uncertainties, test procedure, randomness and inaccuracy when defining the local coordinate system to Formula (4). Once all uncertainties are uncorrelated, the sensitivity coefficient (c_i) is equal to one.

In the following chapter, an uncertainty budget¹⁵ will be used to report the measurement uncertainty.

¹⁵ Uncertainty budget is a table where all information regarding each uncertainty account in the measurement uncertainty can be found. Thus, it summarizes all standard uncertainties, its types and distribution, units and so on (Ball 2014).

4.8 Online Survey¹⁶

The measurement uncertainty acquired before was then, used to enhance the understanding of the quality parameters and consequently the sensor's abilities by adding in the results visualization. Thus, in order to provide reliable graphical representations, an online survey was created to test the efficacy of each representation.

As the quality parameters generated discrete data, with the exception of the PF, mainly 1D plots were created to represent the quality parameters. The survey was shared with 33 people who have a background in Cartography, Geodetics and other majors as Mathematics and Mechanical Engineering. The choice of these majors can be justified once part of them, have a strong knowledge of data and data representation and the other constitute the target audience of this research.

Thus, for the conducted survey, an internet based questionnaire with 18 questions split into three parts was developed. Each parameter was evaluated through two different plots¹⁷. The participants were questioned regarding the illustrations used to visualize the acquired data more specifically, if they were intuitive and immediately understandable or if further information was needed. The choice of questions was made to receive a relevant opinion regarding the chosen visualizations used to plot the accuracy and uncertainty and thus, testing for its effectiveness. The participants were also encouraged to give their opinion of how each visualization could be improved.

4.9 Software used

To compose the results and documentation of this master thesis, the following software packages were necessary.

The following software and tools was used during the elaboration of this master thesis:

- Stand-Alone software: Agisoft PhotoScan Professional 1.3.2.4205
- 3D point cloud processing software: CloudCompare v2.8.1
- 3D modelling software: SketchUp 17.1.174
- Mathematical computing software: Matlab 2015b
- Development cloud-based software: SurveyMonkey
- Office suite: Microsoft Office 2013
- Reference management software: Citavi 5

¹⁶ The online survey was created at the development cloud-based software [SurveyMonkey](#) using a free account. The software was developed by Ryan Finley and is powered by Copyright © 1999-2017 SurveyMonkey

¹⁷ All plots were generated with Matlab 2015b. As a further work, the goal is to integrate both methodologies to a common Script in Matlab.

5 RESULTS AND DISCUSSION

5.1 Accuracy results

In this section, the results for the evaluation and assessment (see 4.6) of the study-case are analyzed. For each system the overall results for each quality parameter is presented as well as, the overall analysis of the results for the evaluation and assessment of the adapted tests.

For the assessment of the system, the MPE of the scan system and the expanded uncertainty for each artefact must be acquired.

The manufacturer provided the MPE value for each scan system. For the Laser Line Scanner $MPE = 5mm$ employed. The laser line sensor is a prototype in its development phase and thus, this is the main reason for the adoption of such value. For the photogrammetric systems I and II a $MPE = 500\mu m$ and a $MPE = 150\mu m$ were employed, respectively.

The expanded uncertainty used on the Probing Error assessment test can be retrieved from Formula (6). For the Laser Line Sensor and photogrammetric system I, U refers to the 70mm sphere, while for the photogrammetric system II to the 38mm sphere. The expanded uncertainty used on the SD and E assessment test can be retrieved from (7). Although these results are already being introduced on the assessment of each quality parameter, its results are provided in 5.2.1 together with the measurement uncertainty analysis.

The detailed evaluation of each scan system comprising the results of the quality parameters for each position is found in the Appendix part (see C) of this research.

5.1.1 Probing Error analysis

The results presented in Table 8 corresponds to the evaluation of the Probing Error parameter and the last column represents the assessment value for each scan system. For the assessment part, the absolute values of each quality parameter and MPE were accounted.

Table 8: Probing Error analysis

	PF μm	PS μm	 MPE - U^{18} μm
Laser Line Scanner	168.7	2430.3	4973.1
Photogrammetric system II (Nikon D610 with AF-S Nikkor 50mm lens)	400.4	477.0	473.1
Photogrammetric system II (Canon 5DSr + Canon 100mm)	13.5	67.2	122.6

¹⁸ This expanded uncertainty (k=2) corresponds to the Probing Error uncertainty that was acquired for the test procedure, as explained in 2.2.3.

The PF quality parameter refers to the ability of each system in measuring form. All values presented in the table corresponds to the mean radial standard deviation of the acquired positions for the respective scan system. All positions of each scan system could be assessed to the PF and therefore, the above values can be used to describe the accuracy of the system.

The PS quality parameter refers to the ability of the sensor in measuring size. The values displayed in the table correspond to the mean value of the acquired positions for the respective scan system. All values with the exception of the second and third positions of the photogrammetric system II could be assessed. One possible contribution of such result can be justified by the chosen coating. Although, the coating was applied uniformly and many features were easily detected during the reconstruction, the glossiness of the sphere was not completely removed. Another possible reason could be the choice of the arbitrary positions within the sensor measuring volume. Although the test is carried to test exactly for these variations, it is important to respect the boundaries of the sensor measuring volume in order to have sharp images. Thus, following the recommendations of the guideline, the measurement for the non-validated positions should be repeated three times.

5.1.2 Sphere-Spacing Error and Length Measurement Error analysis

The results presented in Table 9 present the evaluation of the Sphere Spacing Error and Length Measurement Error where the last column comprises the values for the assessment of the system.

Table 9: Sphere Spacing and Length Measurement Error analysis

	SD μm	E μm	 MPE - U¹⁹ μm
Laser Line Scanner	-490.2	2108.8	4969.8
Photogrammetric system I (Nikon D610 with AF-S Nikkor 50mm lens)	177.8	1055.4	469.8
Photogrammetric system II (Canon 5DSr + Canon 100mm)	115.1	224.8	123.9

The SD quality parameter is used to extract the length in between two spheres. The SD values represented in the above table are the mean value of each acquired position associated to corresponding scan system. All values with the exception of the Position 02 for the photogrammetric system II could be assessed, as described in 4.6.3. The result can be justified due to the wrong detection of the targets used in the definition of the coordinate system. When translating the focus between the spheres (see 4.3.2) the acquired images were not sharp enough thus, affecting considerably the results if compared to the other acquired positions.

The E quality parameter is used to return the error of the length associated to the measurement. The proposed solution considered the evaluation of the parameter through method A due to its simplicity during the acquisition. However, the results proved a tendency to be overestimated. Carmignato,

¹⁹ This expanded uncertainty (k=2) corresponds to the Sphere Spacing Distance uncertainty that was acquired for the test procedure, as explained in 2.2.3.

Savio (2011) pointed that this parameter cannot be easily achieved with photogrammetric approach once the system cannot be reduced to single points. Besides, the authors also highlight that it depends on how the Probing error was derived, the parameter can exert a great influence in the acquisition of E. Therefore, based on the results acquired and specially on the conclusion drawn by Carmignato, Savio (2011) the evaluation of E parameter will be disregarded from this master thesis.

5.2 Measurement uncertainty results

Measurement uncertainty is introduced first on the analysis of the results, once its values are intrinsic to all further considerations. Thus, this section contains the analysis of the measurement uncertainty. First, we provide the results for the test procedure uncertainty as recommended by the guideline (see 2.2.3). The result of the test procedure, in this study case, is only related to the artefact manufacturing. The section then follows with the analysis of the measurement uncertainty according to the GUM specifications. Thus, an uncertainty budget is provided to account for the randomness derived from the quality parameters acquisition together with the test procedure and the inaccuracy when defining the local coordinate system.

5.2.1 Test procedure results

The test procedure results account only for the influence of the artefact on the measurement. By accounting for these values, all external influences on the measurement tend to be minimized. The guideline suggests this approach so, the results achieved are only associated to the acquisition and measurement. Thus, Table 10, Table 11 and Table 12 indicates the results acquired for each quality parameter according to each used sphere during the evaluation. G40 and G28 are used to indicate the quality of the sphere and corresponds to the 70mm and 38mm sphere, respectively.

Table 10: Standard uncertainty Probing Error

Probing Error - $u(p)$	
G40 (μm)	G28 (μm)
19.0	13.7

Table 11: Standard uncertainty Sphere Spacing Error (70mm sphere)

Sphere Spacing Error (G40) - $u(SD)$		
(u) Calibration artefact (μm)	(u) Coating (μm)	(u) Plate (μm)
361.0	225.0	100.0
15.1		

Table 12: Standard uncertainty Sphere Spacing Error (38mm sphere)

Sphere Spacing Error (G28) - $u(SD)$		
(u) Calibration artefact (μm)	(u) Coating (μm)	(u) Plate(μm)
187.7	225.0	100.0
13.1		

5.2.2 Measurement uncertainty analysis

As detailed in 4.7.1.2, the measurement uncertainty recommended by this developed solution, relates uncorrelated uncertainty from three different sources acquired until the pre-processing phase. Thus, following the GUM recommendations, the measurement uncertainty is detailed through an uncertainty budget.

The target uncertainty or the mechanical coordinates of the robot is used to indicate the inaccuracy of the system when defining the coordinate system. Thus this is a fixed value for each scan system where Laser Line sensor present an standard uncertainty of 57,74 μm , the Photogrammetric system I presents a standard uncertainty of 14,43 μm and finally, the photogrammetric system II present a standard uncertainty of 8,66 μm . The values for test procedure are shown in Table 10, Table 11 and Table 12 while the uncertainty associated to each quality parameter was acquired through the measurement evaluation. Thus, PF standard uncertainty is given as the mean value of the acquired positions; PS and SD are given as the standard deviation of the mean.

To account for randomness in the data through three observations proved non-conclusive, once the sample is not representative. Nonetheless, the measurement uncertainty acquired through the GUM specifications constitutes a solid method to account for the measurement uncertainty. Each uncertainty budget was carefully calculated with a proper coverage factor, ensuring a confidence interval of 95%. Thus, the acquired values will be used to compose the accuracy and visualization part of this research.

The detailed evaluation of calculated uncertainty budget, is found in the Appendix part (see D) of this research. The table below illustrates an example of the uncertainty budget acquired for the photogrammetric system II using the PF measurement.

Table 13: Uncertainty Budget using PF acquired from the photogrammetric system II

Canon 5DSr + Canon 100mm - Probing Error Form					
Uncertainty Source	Standard uncertainty	Type	Distribution	Units	DOF
Probing Error Form	13.5	A	Normal	μm	2
Targets uncertainty	8.7	B	Rectangular	μm	infinity
Test procedure	13.7	B	Normal	μm	infinity
Combined standard uncertainty (u)					21.1
Expandend uncertainty (95%) - k=2					42.2

5.3 Online survey results

The online survey had a representative sample of 16 people ($\cong 49\%$). At the beginning of the questionnaire, the respondents were asked about their major. Whence, eight attendee have accomplished a Cartographic study, six attendee a Geodetic study and the further two a physical background.

The survey started with a brief introduction of this master thesis, where the research objective and a description about each quality parameter was provided. It was also highlighted that the data used for each representation was an estimation of the real values and thus, the attendees should consider more the overall visualization instead of analyzing the data itself.

5.3.1 Part I analysis²⁰

Coming to the first part, a scatter bar and an error bar visualization were presented and the attendees were questioned about their understanding about the plots. 75% of the sample were able to understand immediately and 18.75% were able to understand fairly the information displayed in the plots, while only 6.25% was not able to understand it.

When further information was provided in a detailed description text, for 43,75% it helped to improve their understanding of the illustration while 6.25% still remained not understanding. For the remaining 50% this textual information was not required to understand the data in the way it was shown. According to the opinion of 87.5%, the visualizations was rated as a good approach to visualize such data. Thus, through a comparison of the error bar and scatter bar plots, the error bar was preferred by 87.5% of the attendees.

In this step an error was encountered on the description of the parameter, however, once the online survey was based on random values and the given description met the one from the Probing Error Size this visualization will be replaced.

5.3.2 Part II analysis²¹

In the second part, the sample was questioned regarding options to visualize the results for the PS. Therefore, a scatter plot and an onion plot were showed to the sample. 33,33% of the respondents were able to understand immediately and 46,67% fairly what was being presented, while 20% didn't understand and needed more information.

When further information was provided in a detailed textual description, according to 66,67% it improved the understanding of the illustration while for 6,67% the textual description was unclear and for another 6,67% the entire visualization of PS remains unclear. The remaining 20% of the attendees were able to understand the visualization without any additional information.

According to the opinion of 60% of the attendee the data visualized in the illustration could be easily understood, 33,33% saw room for improvements while for 6,67% the proposed way of visualization

²⁰ The analyze results of this part can be checked on [Methodology for evaluation of precision and accuracy of different geometric 3D data acquisition methods](#). This shared page belongs to the online survey created by the master student and is provided by the development cloud-based software SurveyMonkey.

²¹ The analyze results of this part can be checked on [Part II: Probing Error Size \(PS\) analysis](#). This shared page belongs to the online survey created by the master student and is provided by the development cloud-based software SurveyMonkey.

remains unclear. A comparison of onion chart and scattered plot doesn't show a clear preference as 53,33% preferred the onion chart and 46,67% preferred the scattered plot. Thus, the onion chart will be used to represent the mean value of the Probing Error Size parameter.

One person skipped part II of the survey. The visualization displayed was improved with the aid of the captured comments from the online survey.

5.3.3 Part III analysis²²

In the third and last part of this survey, it was presented to the attendees two bar charts where questions about its readability were made. 57,14% were able to understand the charts immediately while 35,71% had a fairly understanding. 7,14% could not understand the illustration.

Then, a textual description in order to improve the graphs readability was provided. It was found that 78,57% required the description to understand the illustration while for the remaining 21,43% this description was not even necessary.

The overall summary of this part concluded that 71,43% considered the created charts a good representation to visualize and compare accuracy + uncertainty. 14,29% stated that the visualizations could be improved while the remaining 14,29% preferred a different visualization. A comparison between the two illustrations showed that the Stacked bar chart was preferred by 61,54%.

In this survey, the visualization of the dispersion points compared to its theoretical surface was also provided and the audience were questioned about its efficacy and added value on what is being evaluated. 57,14% of the attendees considered that its display can assuredly be beneficial and the readability could be perceived immediately by 64,29% of the attendees.

Two people skipped this part of the survey. All comments given for improvement were captured and used to improve the visualizations in this master thesis.

5.3.4 Overall analysis

According to the online survey, the representations created to visualize the measurement uncertainty can aid the users to improve their understanding of the evaluated scan system. It is important to highlight that the objective of this online survey was merely to test the readability of the created visualizations and to assure that the user can benefit from such.

5.4 Measurement uncertainty visualization results

5.4.1 Probing Error Form visualization

The Probing Error Form can be visualized by plotting the radial deviation from the 3D coordinates to its theoretical surface, the best-fit sphere represented as a gray color. Thus, the visualization indicated

²² The analyze results of this part can be checked on [Part III: Sphere-Spacing Error and Dispersion Plot](#). This shared page belongs to the online survey created by the master student and is provided by the development cloud-based software SurveyMonkey.

by Figure 17 provides a good overview of the ability of each scan system. These visualizations were generated with the Matlab and compose the overall solution suggested in this master thesis.

To generate such plot, the 3D coordinate and the radial deviation of each represented position is necessary. The radial error is then projected from its respective coordinate to the best fit. Such behavior can be more easily perceived in the representation of the photogrammetric system I. To allow comparison between the scan systems, the plots were generated using the same interval. The points were partitioned in six different groups, using a quartile function. The partition of the point cloud allows a better and easier interpretation of the intrinsic behavior of each system. The color bar indicates the maximum and minimum of the interval as well as the clustering values.

The measurement uncertainty was not indicated in this visualization, once it was not possible to create a simple visualization using uncertainty without adding more uncertainty to the data. As the range of points was varying from a few hundred thousand to some millions of points, such visualization proved to be impractical. Therefore, only the radial deviation is being visualized.

5.4.2 Probing Error Size visualization

The visualization created by the PS represents the measurement uncertainty. Thus, two visualizations are being displayed, one containing the scatter error plot of the diameter and the other associating the range of the measurement uncertainty to its diameter.

The visualization using the circular representation, similar to an onion plot, is being represented through the mean diameter, the measurement uncertainty interval and the calibrated diameter. The circle's center has an opaque color, since it is an area where the uncertainty does not interfere. As the overall result of PS is given as a mean value, the visualization is a good approach to visualize the confidence interval. Thus, Figure 18 contains the visualization of all scanning systems tested in this master thesis.

The second visualization is a scatter error plot (Figure 19), here illustrated only by the photogrammetric system I. Such representation proves to be better when the analysis of each measurement uncertainty is aimed. However, once measurement uncertainty is based on the standard deviation of the mean, all error plots are of the same size and thus masking the uncertainty of the certain position.

The visualizations generated for the PS parameter compose the solution of this master thesis, and was created with Matlab.

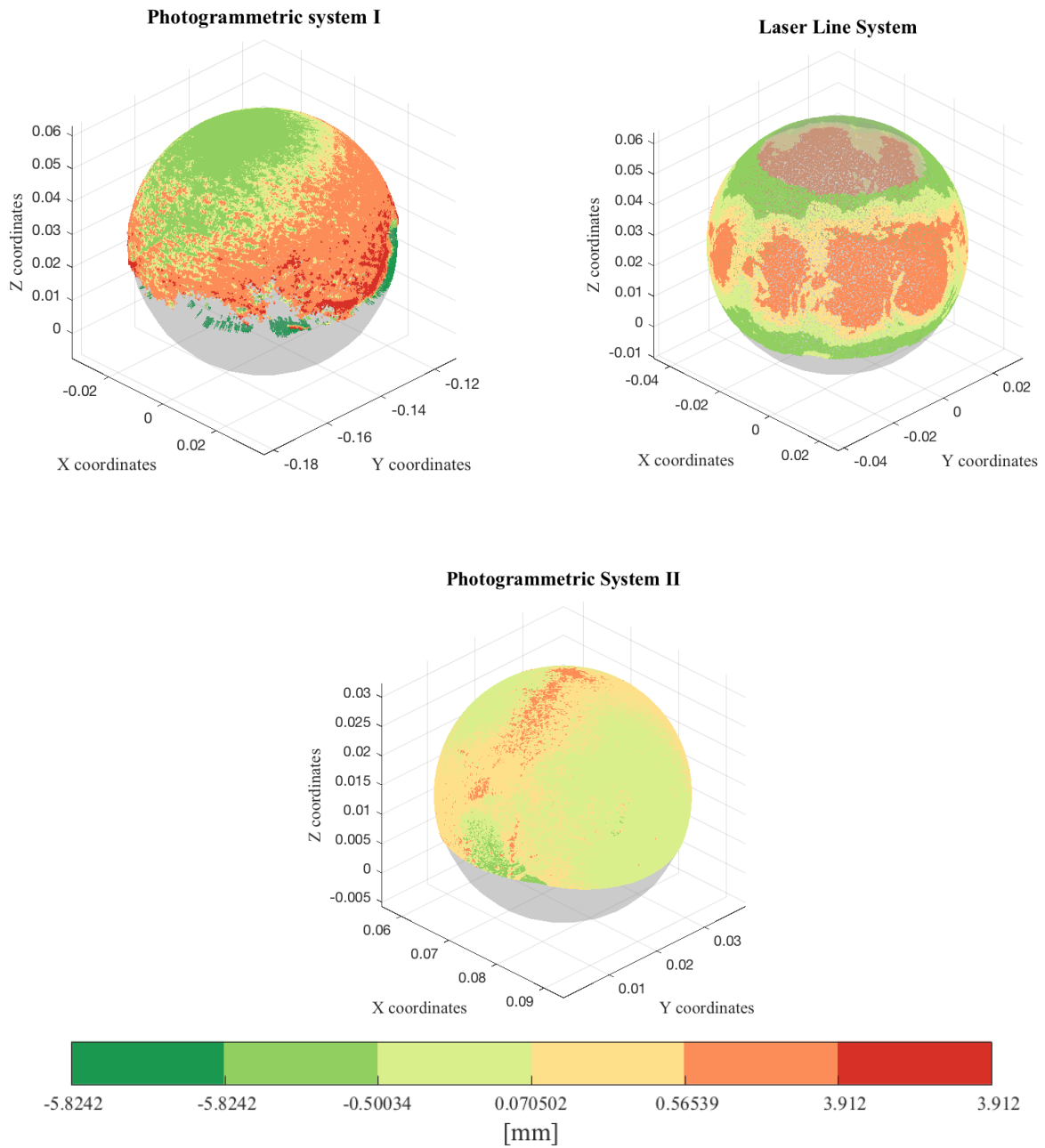


Figure 17: Radial dispersion visualization for each evaluated scan systems (generated with Matlab)²³

²³ The color scheme used in the plots of this research was acquired from the FEX of Matlab. The function is named [cbrewer](#) and is licensed under Copyright (c) 2015, Charles Robert.

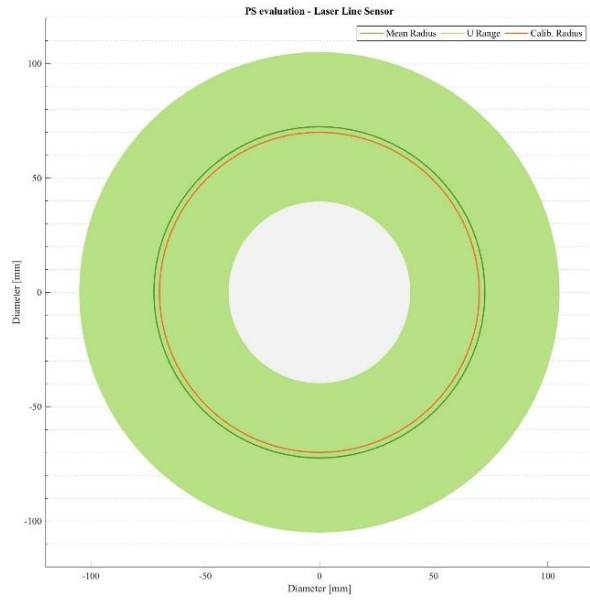
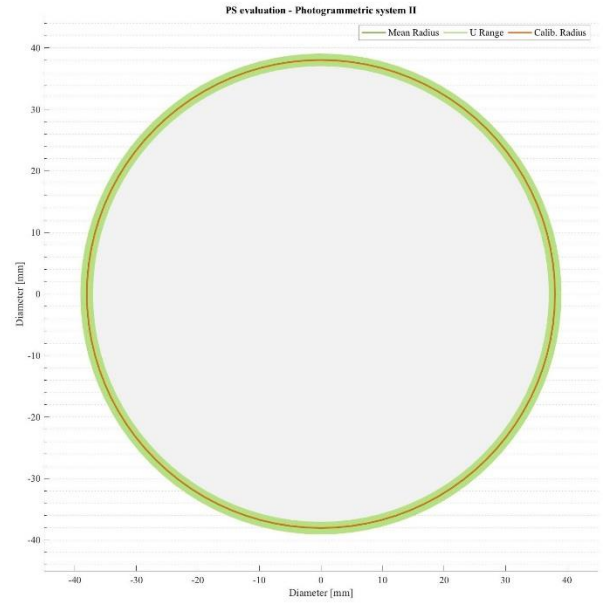
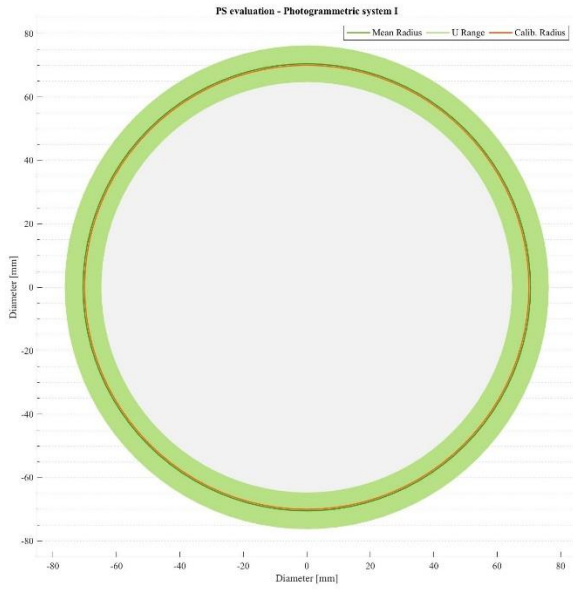


Figure 18: PS evaluation based on the mean value, created with Matlab

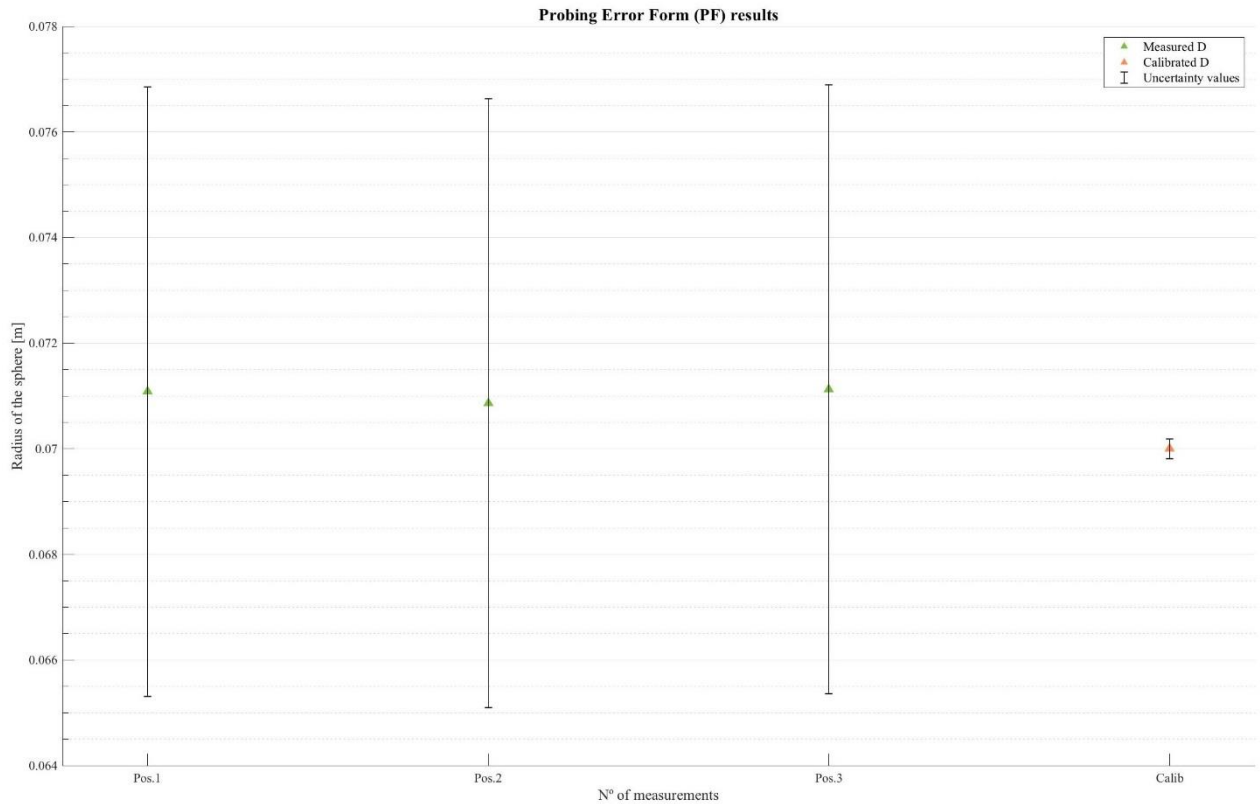


Figure 19: SD evaluation of each position for the Nikon D610 with AF-S Nikkor 50mm lens (created with Matlab)

5.4.3 Sphere Spacing Error visualization

The visualization generated for the SD parameter is a stacked bar chart where the user not only can perceive the measurement uncertainty but also, compare the ability of the scan in measuring the distance between two centers.

When the uncertainty is very small, the measurement uncertainty will be probably not easily distinguished in the main visualization. Therefore, for systems that the difference are so small that cannot be perceived in the main plot a magnification screen is displayed under the legend. This representation was preferred over truncate the axis above zero once, by providing all information about the measured lengths the user can improve the readability not only of the visualization but consequently from the scan system.

The visualizations generated for the SD parameter compose the solution of this master thesis, and were created with Matlab.

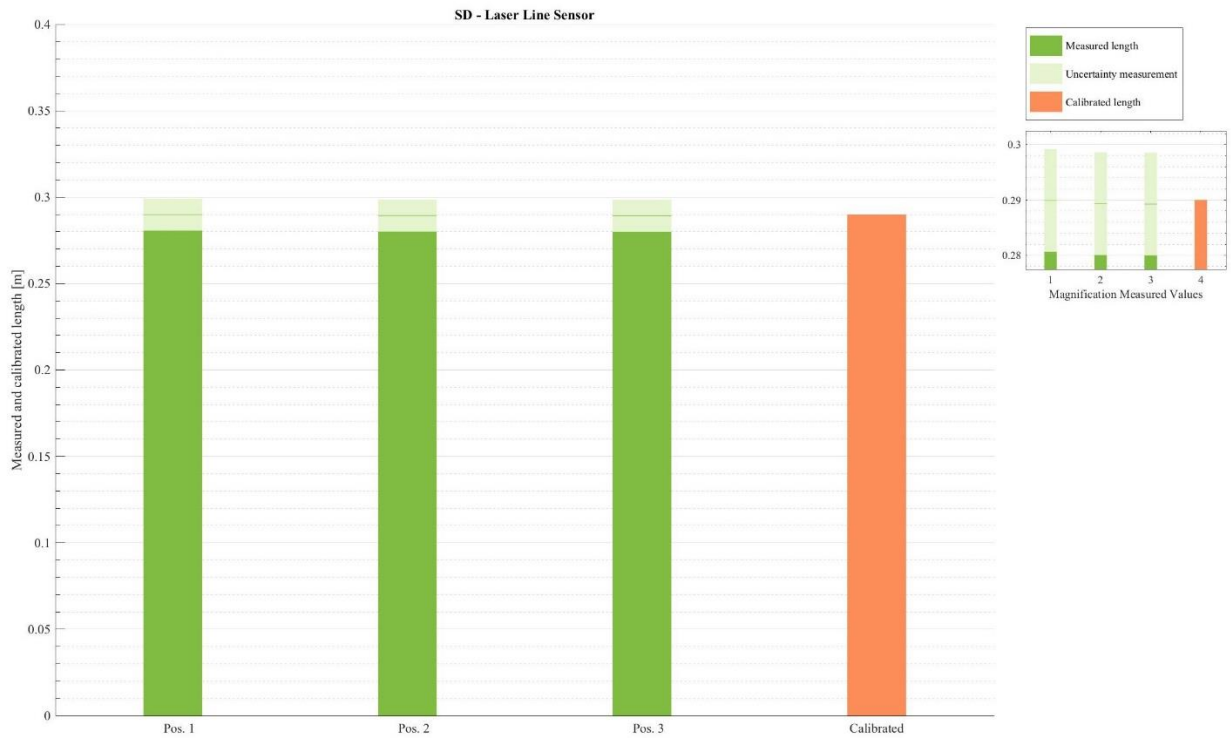


Figure 20: SD evaluation for each position of the Laser Line Scanner, created with Matlab²⁴

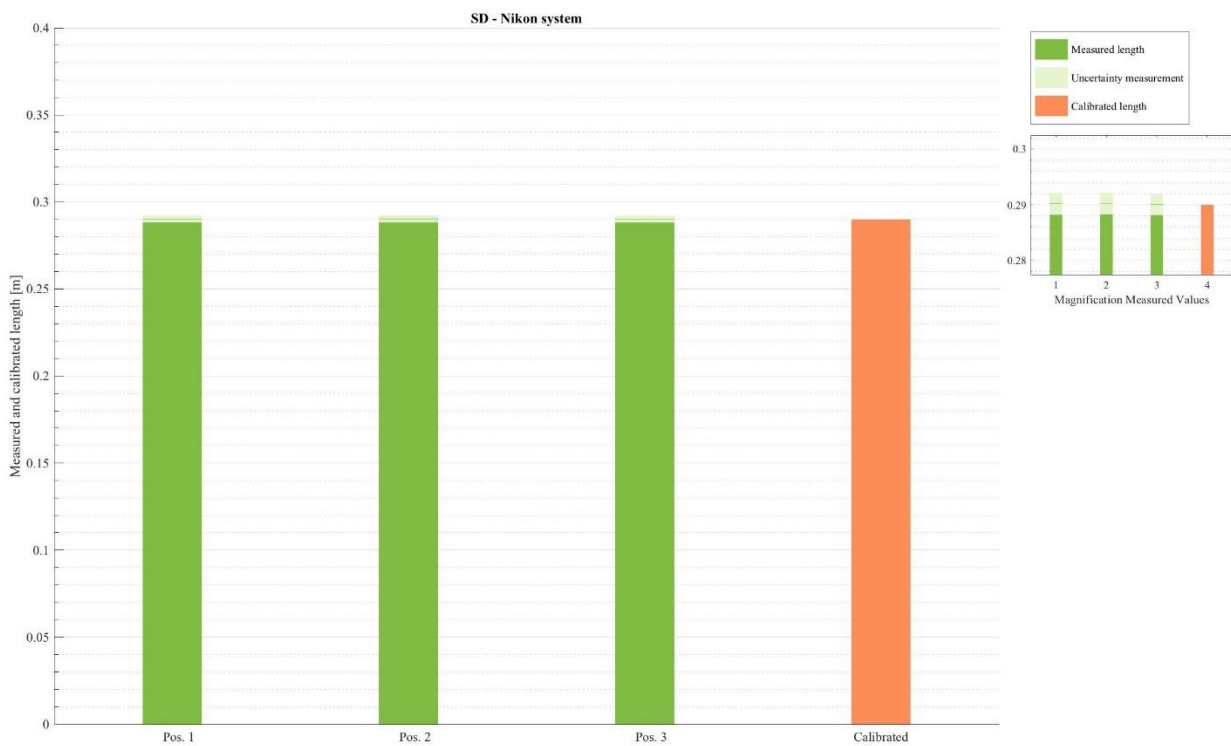


Figure 21: SD evaluation for each position of the Nikon D610 with AF-S Nikkor 50mm lens, created with Matlab

²⁴ Besides the use of the cbrewer FEX, these plots were also create with the aid of another FEX of Matlab. The function is named [freezeColors / unfreezeColors](#) and is license under Copyright (c) 2017, John Iversen

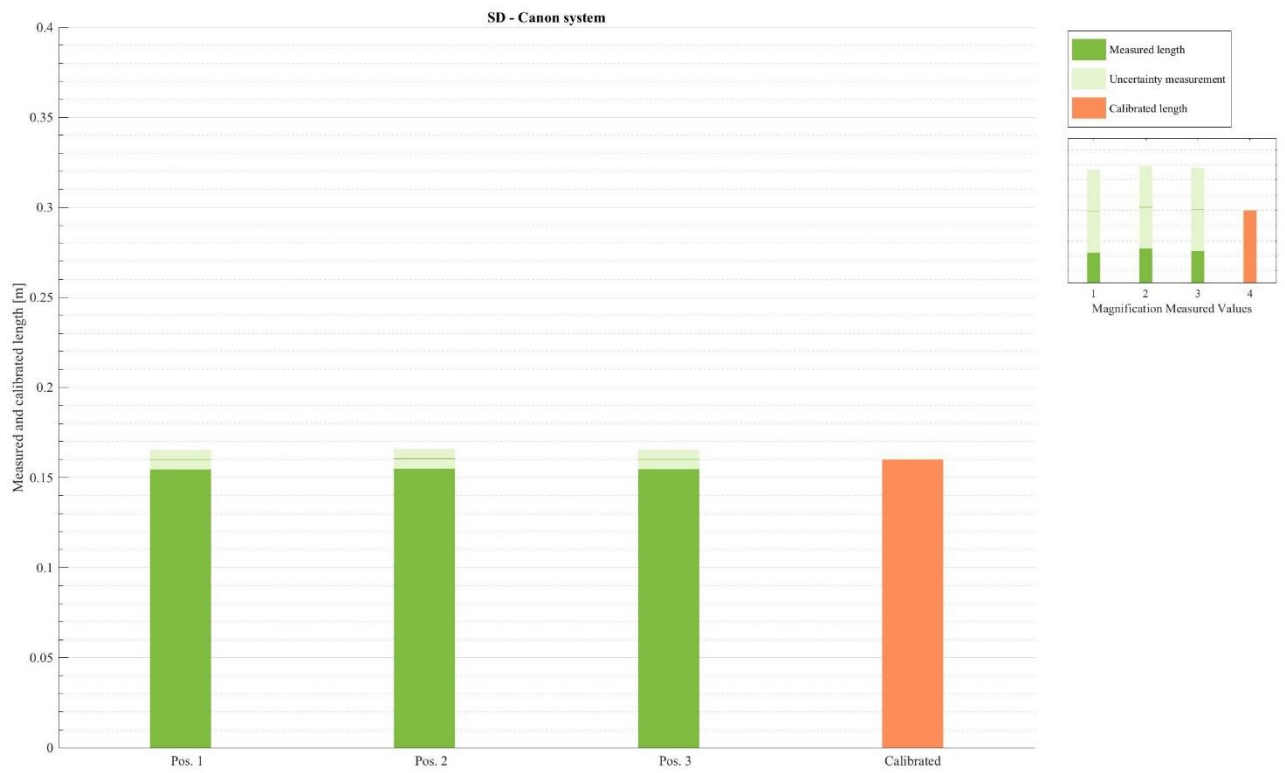


Figure 22: SD evaluation for each position of the Canon 5DSr + Canon 100mm lens, created with Matlab

6 CONCLUSION AND FURTHER WORK

This master thesis aimed to develop a general solution to assess accuracy for different optical 3D scanning systems and its visualization. Thus, its evaluation is based on the principles provided by the VDI/VDE 2634 Part 3 and covers all steps from the acquisition to the visualization of the results to achieve comprehensible representations and to improve the user readability.

To meet the objective of this master thesis, an extensive research was required. First, a calculation model for the assessment of accuracy of optical 3D scanning systems based on the guideline recommendations was developed. Thus deriving a best-fit algorithm and the functions that can extract from it, and each quality parameter.

In a second step, the developed model was evaluated with an experimental setup. Therefore, calibrated artefact and adapted test was prepared accordingly. The adapted test was performed in collaboration with Fraunhofer IGD, the study-case of this research. Thus, under a controlled testing environment three different sensors including one prototype were evaluated. The results from each evaluation proved that different sensors can be assessed by the adapted test and reliable results can be extracted with the aid of the calculation model. The algorithm showed good performance when deriving data from different systems and thus, point clouds varying from a few hundred thousands to millions of points can be easily calculated.

In a further step, the sources of uncertainty that could directly affect the measurement were identified. The uncertainties were then accounted for the measurement uncertainty.

Finally, the results extracted from the algorithm associated to the measurement uncertainty were then, used within a visual evaluation of each parameter. Therefore various appropriate ways of visualization were developed. As discrete data was generated, the choices of representations were limited and thus an online survey was created. According to the survey, the chosen plots proved to enhance the user readability of the generated data.

The developed solution was applied to different scan systems and reliable results were extracted from the evaluated technologies. Thus, based on the described work of this thesis the developed solution can be applied to any system that complies with the VDI/VDE 2634 Part 3. However, this solution is based on a photogrammetric system and thus, the quality parameter acquisition can be even more laborious than the one defined by the guideline.

Although the plausibility of the achieved data was proven by multiple testing iterations and the use of three different equipment, the influence of some factors need to be further analyzed: For the surface treatment of the measured artefacts, a new coating property should be analyzed. Although, the coating used in this research was able to acquire good results, the glossiness of the sphere was not completely removed and such influence could be detected on the measurement.

Besides, when accuracy is expected as a final result, the user must have control of every variable that can affect the system. Thus, accounting for uncertainty is crucial. The method proposed here followed the specification of the GUM guide, which proved to be a straightforward solution when accounting for different sources of uncertainty. However, without introducing repeatability into the measurement the randomness cannot be precisely defined.

The proposed solution proved to consider all aspects of the measurement, starting from its preparation and going all the way to its visual representation. As it can be easily recreated, this solution can be applied for experienced and non-experienced users. Furthermore, it allows to provide a precise overview of the system's capability. Thus, the findings achieved during this research are an important step towards the assessment of the accuracy and the visualization of measurement uncertainty, however, various factors effecting the accuracy were not investigated and thus further refinements must be employed.

BIBLIOGRAPHY

- Acko, Bojan; McCarthy, Michael; Haertig, Frank; Buchmeister, Borut (2012): Standards for testing freeform measurement capability of optical and tactile coordinate measuring machines. In *Meas. Sci. Technol.* 23 (9), p. 94013. DOI: 10.1088/0957-0233/23/9/094013.
- Agisoft LLC (2017): Agisoft PhotoScan User Manual: Professional Edition, Version 1.3. Available online at http://www.agisoft.com/pdf/photoscan-pro_1_3_en.pdf, checked on November 10th, 2017.
- Ball, John (2014): G104- Guide for Estimation of Measurement Uncertainty in Testing. American Association for Laboratory Accreditation (A2LA)). Available online at https://portal.a2la.org/guidance/est_mu_testing.pdf, checked on December 02th, 2017.
- Barbero, Basilio Ramos; Ureta, Elena Santos (2011): Comparative study of different digitization techniques and their accuracy. In *Computer-Aided Design* 43 (2), pp. 188–206. DOI: 10.1016/j.cad.2010.11.005.
- Beraldin, J.-A.; El-Hakim, Sabry; Cournoyer, Luc; Picard, M. (2007b): Traceable 3D Imaging Metrology: Evaluation of 3D Digitizing Techniques in a Dedicated Metrology Laboratory, pp. 310–318.
- Beraldin, J.-Angelo; Carrier, Benjamin; Mackinnon, David Kenneth; Cournoyer, Luc (2012): Characterization of triangulation-based 3D imaging systems using certified artifacts. In *NSCLI Measure*. Available online at <https://www.researchgate.net/publication/235707865>.
- Beraldin, J.-Angelo; Mackinnon, David; Cournoyer, Luc (2015): Metrological characterization of 3D imaging systems. Progress report on standards developments. In Bernard Larquier (Ed.): 17th International Congress of Metrology. 17th International Congress of Metrology. Paris, France, September 21-24, 2015. Les Ulis, France: EDP Sciences, p. 13003.
- Beraldin, J.-Angelo; Rioux, Marc; Cournoyer, Luc; Blais, Francois; Picard, Michel; Pekelsky, Jim (2007a): Traceable 3D imaging metrology, 64910B. DOI: 10.1117/12.698381.
- Bernardini, Fausto; Rushmeier, Holly (2002): The 3D Model Acquisition Pipeline. In *Computer Graphics Forum* 21 (2), pp. 149–172. DOI: 10.1111/1467-8659.00574.
- BIPM (2008): International vocabulary of metrology - Basic and general concepts and associated terms (VIM). JCGM 200:2012(E/F).
- Blais, François (2004): Review of 20 years of range sensor development. In *J. Electron. Imaging* 13 (1), p. 231. DOI: 10.1117/1.1631921.
- Bonneau, Georges-Pierre; Hege, Hans-Christian; Johnson, Chris R.; Oliveira, Manuel M.; Potter, Kristin; Rheingans, Penny; Schultz, Thomas (2014): Overview and State-of-the-Art of Uncertainty Visualization. In: Hansen C., Chen M., Johnson c., Kaufman A., Hagen H. (eds) *Scientific Visualization*: Springer, London.

- Brodlie, Ken; Allendes Osorio, Rodolfo; Lopes, Adriano (2012): A Review of Uncertainty in Data Visualization. In: Dill J., Earnshaw R., Kasik D., Vince J., Wong P. (eds) *Expanding the Frontiers of Visual Analytics and Visualization.*: Springer, London.
- Carmignato, Simone; Savio, Enrico (2011): Metrological performance verification of coordinate measuring systems with optical distance sensors. In *IJPTECH* 2 (2/3), p. 153. DOI: 10.1504/IJPTECH.2011.039457.
- DxOMark (2017): Introducing DxOMark. Available online at <https://www.dxomark.com/about-us>, checked on November 18th, 2017.
- Farrance, I., & Frenkel, R. (2012): Uncertainty of Measurement: A Review of the Rules for Calculating Uncertainty Components through Functional Relationships. In *The Clinical Biochemist Reviews* 33(2), 49–75. Available online at <https://www.ncbi.nlm.nih.gov/pmc/articles/PMC3387884/>.
- Forbes, A. B. (1989): Least squares best fit geometric elements. National Physical Laboratory (NPL). United Kingdom (NPL Report DITC 140/89).
- Geodetic Systems (n.d): What is Photogrammetry? Available online at <https://www.geodetic.com/v-stars/what-is-photogrammetry/>, checked on October 4th, 2017.
- DIN ISO/TS 23165:2008-08: Geometrical product specifications (GPS) - Guidelines for the evaluation of coordinate measuring machine (CMM) test uncertainty (ISO/TS 23165:2006).
- Grigoryan, Gevorg; Rheingans, Penny (2004): Probabilistic Surfaces: Point Based Primitives to Show Surface Uncertainty. In *IEEE transactions on visualization and computer graphics* Vol. 10, No. 5, pp. 564–573.
- Guidi, Gabriele; Russo, Michele; Magrassi, Grazia; Bordegoni, Monica (2010): Performance evaluation of triangulation based range sensors. In *Sensors (Basel, Switzerland)* 10 (8), pp. 7192–7215. DOI: 10.3390/s100807192.
- JCGM (2008): Evaluation of measurement data - Guide to the expression of uncertainty in measurement - JCGM 100:2008. (GUM 1995 with minor corrections).
- Jekel, C. (2015): Least Squares Sphere Fit. Available online at <http://jekel.me/2015/Least-Squares-Sphere-Fit/>, updated on 9/13/2015, checked on July, 2017.
- Joshi, Prateek (2014): Understanding Camera Calibration. Perpetual Enigma. Available online at <https://prateekvjoshi.com/2014/05/31/understanding-camera-calibration/>, updated on 2014, checked on October 6th, 2017.
- Lerma, José Luis; Navarro, Santiago; Cabrelles, Miriam; Villaverde, Valentín (2010): Terrestrial laser scanning and close range photogrammetry for 3D archaeological documentation. The Upper Palaeolithic Cave of Parpalló as a case study. In *Journal of Archaeological Science* 37 (3), pp. 499–507. DOI: 10.1016/j.jas.2009.10.011.
- Lima, C. R. G. (July 10th, 2006): Um estudo comparativo de sistemas de medição aplicáveis ao controle dimensional de superfícies livres em peças de médio e grande porte. Master Thesis. Federal

University of Santa Catarina, Florianópolis, Brazil. Pós-MCI. Available online at <http://repositorio.ufsc.br/xmlui/handle/123456789/88711>, checked on October 2nd, 2017.

Liu, Wen-Cheng; Huang, Wei-Che (2016): CLOSE RANGE DIGITAL PHOTOGRAMMETRY APPLIED TO TOPOGRAPHY AND LANDSLIDE MEASUREMENTS. In *Int. Arch. Photogramm. Remote Sens. Spatial Inf. Sci.* XLI-B5, pp. 875–880. DOI: 10.5194/isprsarchives-XLI-B5-875-2016.

Luhmann, Thomas; Robson, Stuart; Kyle, Stephen; Boehm, Jan (2014): Close-range photogrammetry and 3D imaging. 2nd edition. Berlin: De Gruyter (De Gruyter textbook).

MathWorks (2017): What is camera calibration? Available online at <https://de.mathworks.com/help/vision/ug/camera-calibration.html>, checked on October 7th, 2017.

Matthews, N. A. (2008): Aerial and Close-Range Photogrammetric Technology: Providing Resource Documentation, Interpretation, and Preservation. Technical Note 428. Denver, Colorado, United States of America. Available online at <https://www.blm.gov/nstc/library/pdf/TN428.pdf>, checked on October 3rd, 2017.

Mendricky, Radomir (2016): Determination of measurement accuracy of optical 3D scanners. In *MM SJ* 2016 (06), pp. 1565–1572. DOI: 10.17973/MMSJ.2016_12_2016183.

Moons, Theo.; van Gool, Luc; Vergauwen, Maarten (2008): 3D Reconstruction from Multiple Images Part 1: Principles (4), checked on October 8th, 2017.

NDT Resource Center (n.d): Accuracy, Error, Precision, and Uncertainty. With assistance of NSF-ATE (Advanced Technological Education) program. Available online at <https://www.nde-ed.org/GeneralResources/ErrorAnalysis/UncertaintyTerms.htm>, checked on November 26th, 2017.

Pang, Alex T.; Wittenbrink, Craig M.; Lodha, Suresh K. (1996): Approaches to Uncertainty Visualization. University of California. Santa Cruz, CA, USA. Available online at <https://www.soe.ucsc.edu/sites/default/files/technical-reports/UCSC-CRL-96-21.pdf>.

Panyam, Meghashyam (2007): Least Squares Fitting of Analytic Primitives on a GPU. Master of Science Mechanical Engineering. Clemson University, South Carolina, USA. Available online at http://tigerprints.clemson.edu/cgi/viewcontent.cgi?article=1232&context=all_theses.

Pöthkow, Kai; Hege, Hans-Christian (2011): Positional Uncertainty of Isocontours: Condition Analysis and Probabilistic Measures. In *IEEE transactions on visualization and computer graphics* Volume: 17, Issue: 10. DOI: 10.1109/TVCG.2010.247.

RGPBALLS (2017): DIN 5401 International Standards. Available online at <http://www.rgpballs.com/de/products/KUGELN/INTERNATIONALE-NORMEN/toleranzen-der-kugeln-normen-din-5401>, checked on November 22th, 2017.

Robson, Stuart; Beraldin, Angelo; Brownhill, Andrew; MacDonald, Lindsay (2011): Artefacts for optical surface measurement. In *National Research Council Canada (NRC-CNRC); NRC Institute for Information Technology* 8085. Available online at <http://nparc.cisti-icist.nrc-cnrc.gc.ca/eng/view/object/?id=9e97cfa8-2580-442d-b8ce-641f63cb0943>.

Sanyal, Jibonananda; Zhang, Song; Bhattacharya, Gargi; Amburn, Phil; Moorhead, Robert J. (2009): A user study to compare four uncertainty visualization methods for 1D and 2D datasets. In *IEEE*

transactions on visualization and computer graphics 15 (6), pp. 1209–1218. DOI: 10.1109/TVCG.2009.114.

Schmidt, G. S.; Chen, Sue-Ling; Bryden, A. N.; Livingston, M. A.; Rosenblum, L. J.; Osborn, B. R. (2004): Multidimensional Visual Representations for Underwater Environmental Uncertainty. In *IEEE Comput. Grap. Appl.* 24 (5), pp. 56–65. DOI: 10.1109/MCG.2004.35.

Sims-Waterhouse, Danny; Piano, Samanta; Leach, Richard (2017): Verification of micro-scale photogrammetry for smooth three-dimensional object measurement. In *Meas. Sci. Technol.* 28 (5), pp. 1–7. DOI: 10.1088/1361-6501/aa6364.

SMARTTECH 3D scanners (n.d): FAQ: Measurement Volume. Available online at <http://smarttech3dscanner.com/3d-scanning-glossary/measurement-volume/>, checked on November 10th, 2017.

Snavely, N. Keith (2008): Scene reconstruction and visualization from internet photo collections. Doctoral Dissertation. Computer Science & Engineering, Washington. University of Washington. Available online at <http://grail.cs.washington.edu/wp-content/uploads/2015/10/SnavelyPhd.pdf>, checked on October 14th, 2017.

Stadek, Jerzy A. (2015): *Coordinate Metrology: Accuracy of Systems and Measurements*: Springer-Verlag Berlin Heidelberg.

van der Laan, D.; Jonge, Edwin de; Solcer, Jessica (2015): Effect of Displaying Uncertainty in Line and Bar Charts - Presentation and Interpretation, pp. 225–232. DOI: 10.5220/0005300702250232.

VDI (2017): VDI/VDE Society Measurement and Automatic Control. Available online at <http://www.vdi.eu/engineering/vdi-societies/measurement-and-automatic-control/measurement-and-automatic-control/>, checked on November 10th, 2017.

VDI/VDE 2634 Part 2, 2012: VDI/VDE 2634, Part 2. Optical systems based on area scanning.

VDI/VDE 2634 Part 3, 2008: VDI/VDE 2634, Part 3. Optical 3D-measuring systems Multiple view systems based on area scanning.

Westoby, M. J.; Brasington, J.; Glasser, N. F.; Hambrey, M. J.; Reynolds, J. M. (2012): ‘Structure-from-Motion’ photogrammetry. A low-cost, effective tool for geoscience applications. In *Geomorphology* 179, pp. 300–314. DOI: 10.1016/j.geomorph.2012.08.021.

Yilmaz, H. M.; Yakar, M.; Gulec, S. A.; Dulgerler, O. N. (2007): Importance of digital close-range photogrammetry in documentation of cultural heritage. In *Journal of Cultural Heritage* 8 (4), pp. 428–433. DOI: 10.1016/j.culher.2007.07.004.

Zhang, Huijie; Qu, Dezhan; Liu, Quanle; Shang, Qi; Hou, Yafang; Shen, Han-Wei (2017): Uncertainty visualization for variable associations analysis. In *Vis Comput* 12 (5), p. 917. DOI: 10.1007/s00371-017-1359-8.

APPENDIX

A Sensor Measuring Volume and Measurement Volume

a. Sensor Measuring Volume

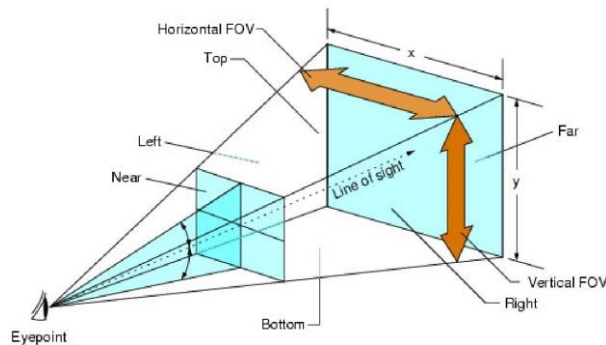


Figure 23: Sensor measuring of the systems under test volume (OpenGL Performer²⁵)

The sensor measuring volume of an image is defined as the volume measured in a single image (VDI/VDE 2634 Part 3 2008), and it is specified by the sensor of the scanning system. For both systems under test, the field-of-view and the depth-of-field of the camera define it. As these values can be very subjective to the camera settings and from the object-sensor distance, the sensor measuring volume used during the measurement of the accuracy should be stated by the manufacturer. Figure 03, presents a schematic representation of the sensor measuring volume.

Field-of-view (FOV) defines the encompassed area in the image and is distance dependent from the sensor to the object. FOV can be determined from the focal length, sensor size and as already mentioned from the distance (Geodetic Systems n.d; Panavision²⁶ 2015). The horizontal and vertical FOV will define the width and height of the image, respectively (Panavision 2015).

The depth-of-field defines how much of the image will appear sharp. Depth-of-field is a function of the focal length and the aperture of the used camera (Panavision 2015; Fleming 2002²⁷) and defines the near and far plane of the image (Fleming 2002).

²⁵ OpenGL Performer™: Getting Started Guide Chapter 4. Introduction to OpenGL Performer Concepts. Getting Started Guide Part II. Programming with OpenGL Performer (Document Number: 007-3560-005). Available online at [OpenGL Performer](#), checked on October 19th, 2017.

²⁶ Panavision (2015): Primo 70 Series. Sensor Size & Field of View. Available online at [Primo 70 series](#), checked on October 20th, 2017.

²⁷ Fleming, Don (2002): Depth of Field Definitions. Available online at [DOFMaster](#), checked on October 26th, 2017.

b. Measurement volume

Measurement volume is defined by the set of images that define the volume of the measured object (VDI/VDE 2634 Part 3, 2008). In other words, measurement volume define, theoretically, the limiting area for the scan system (Mendricky 2016; SMARTTECH 3D scanners n.d).

The measurement volume is dependent on object that are commonly measured or according to the purpose that the scan was developed. However, as in photogrammetric applications this volume can be very flexible, assuming different sizes for different objects. Therefore, the value should be state by the manufacturer (VDI/VDE 2634 Part 3, 2008).

B Best-fit algorithm and Script

a. sphereFit function

This part was created based on the [Least Square Sphere Fit](#) of Charles Jekel and on the function [Sphere Fit](#) of Prem Rachakonda.

```
%This first part is used to define the initial estimatives. Therefore,
%this function does not minimize the sum.
%It is based on the code of the Charles Jekel and Prem Rachakonda and can
%found at <http://jekel.me/2015/Least-Squares-Sphere-Fit/> and
%<https://www.mathworks.com/matlabcentral/fileexchange/45910-sphere-fit>,
%respectively.

function [a,b,c,r] = sphereFit(data)
%Defining the input coordinates x, y, z
sqx = data(:,1);
sqy = data(:,2);
sqz = data(:,3);

%Defining the A matrix
A(:,1)=2*sqx;
A(:,2)=2*sqy;
A(:,3)=2*sqz;
A(:,4)=ones(size(sqx));

%Defining the vector B (using element-wise multiplication)
B=(sqx.*sqx)+(sqy.*sqy)+(sqz.*sqz);

%Solving the linear equation to find the vector X. The following operation
%is the same as making X=inv(A.'*A)*A.'*B. However, the backlash provide
%more stables result in Matlab.
X=A\B;

%Defining the inital estimative for the center point
a=X(1);
b=X(2);
c=X(3);
D=X(4);

%Defining the inital estimative for the radius
r=sqrt(a^2+b^2+c^2+D);

end
```

b. Radial error function

```
%Function to calculate the radial error of each point in the sphere
%By using the deltari=sqrt((xi-a)^2+(yi-b)^2+(zi-r)^2)-r up to 3% of the
%greatest values can be eliminated. After removing the sphre fit should be
%processed again.

%Using the quantile function to retrieve the greatest values

function [output, di]= radial_error (data)

sqx= data(:,1);
sqy= data(:,2);
sqz= data(:,3);

[a0, b0, c0, r0]=sphereFit(data);
```

```

xi= sqx-a0;
yi= sqy-b0;
zi= sqz-c0;
ri=sqrt(xi.^2+yi.^2+zi.^2);

di=ri-r0;

%By using quantile 99.97%, I have the 0.003% of the greatest values. It was
%considered the absolute values since we want to consider positive and
%negative values in module.
threshold = quantile (abs(di), 0.9997);

%Defining the greatest values of the radial error
%q=di(abs(di(:,1))>threshold);

%Defining the variable pos, to allocate the positions
pos =[];

%Loop to locating the position of the rows in the data file where the values
%are bigger than the threshold. The positions will be stored in the pos
%vector
for i = (1:length(sqx))

    if(di(i)>= threshold || di(i) <= -threshold)
        pos=[pos;i];
    end
end

% Function to remove and update the length of the data file, based on the
% position of the greatest values.
output=kick_out(pos, data);

function [out] = kick_out(positions,data_input)
    for i = (1: length(positions))
        data_input =[data_input(1:positions(i)-(i-1)-1,:);data_input(positions(i)-(i-1)+1:end,:)];
        out=data_input;
    end
end
end
end

```

c. Minimization

This part was created based on Forbes (1989) article also cited in this master thesis. The tolerance value followed a similar approach as the one adopted in Panyam (2007) master thesis.

```

%Using the data calculated from the radial error function, the Gauss Newton
%will be used to provide a final estimation for the center and radius.

function [a,b,c, Radius,di]= minimization(output)

%Entry of the 3D coordinates provenient from the .csv file for each sphere

sqx = output(:,1);

sqy = output(:,2);

sqz = output(:,3);

% sq = data(:);

```

```

%Retriving the initial estimated based on the new matrix created after
%removal of the greatest radial errors

[a0,b0,c0,r0]=sphereFit(output);

%For the minimization part the Gauss Newton method will be used.
%It is know that the distance beteween each point on the surface
%and the center returns the radius. According to Alistair Barricleae
%Forbes,"Least-squares best-fit geometric elements" (1991), the
%function that will be minimized is  $d_i=r_i-r$ .

%Findind the  $d_i$  vector

xi= sqx-a0;
yi= sqy-b0;
zi= sqz-c0;
ri=sqrt(xi.^2+yi.^2+zi.^2);
di=ri-r0;

%Defining the Jacobian matrix

J(:,1)=- (xi) ./ri;
J(:,2)=- (yi) ./ri;
J(:,3)=- (zi) ./ri;
J(:,4)=- (ones(size(sqx)));

%Solving the linear system  $Jp=-d_i$  to find the residual vector (p)

p=J\ -di;

%Incrementing the parameters with the residuals

a=a0+p(1);
b=b0+p(2);
c=c0+p(3);
Radius=r0+p(4);

%Based on the Panyam mohan ram, Meghashyam, "Least Squares Fitting
%of Analytic Primitives on a GPU" (2007), a certain tolerance was
%defined and the sum of the residuals, convergence condition, was

```

```

%compared to this value. Therefore, the convergence is reached when
%convergence <= tolerance.

% %Defining the convergence and the tolerance criteria
convergence=abs(p(1)+p(2)+p(3)+p(4));

tolerance = 10e-6;%the data

%Iteration function in case the convergence is not reached

i=0;

if(convergence>tolerance)

    conv=convergence;

    %While loop to upadte the values (center and radius) at each interation
    %and pass to them as input to the sub-function

    while conv>tolerance

        conv = crite2(a,b,c,Radius,di);

        i=i+1; %Number of interations necessary to comply with the tolerance

    end

end

%Sub-function to calculate the new center and radius based on the input
%provided by the while lopp above

function [conv] = crite2(t,u,v,wr,dist)

    %Defining the new the di vector

    xi= sqx-t;

    yi= sqy-u;

    zi= sqz-v;

    ri=sqrt(xi.^2+yi.^2+zi.^2);

    dist=ri-wr;

    %Defining the new Jacobian matrix

    J(:,1)=- (xi)./ri;

    J(:,2)=- (yi)./ri;

    J(:,3)=- (zi)./ri;

```

```

J(:,4)=- (ones (size (sqx)) );

%Finding the updates residual values

q=J\(-dist);

%Incremented values

t=t+q(1);

u=u+q(2);

v=v+q(3);

wr=wr+q(4);

%Checking if the convergence is reached

conv=abs (q (1) +q (2) +q (3) +q (4) );

%Updated values

a=t;

b=u;

c=v;

Radius=wr;

dist=di;

end

end

```

d. Script

Script to run the the best-fit algorithm and acquire the results of each quality parameter. The initial part of this Script was retrieve from [Matlab Wiki](#) and the content is available under the [CC BY-NC-ND 3.0](#) license.

➤ Script to extract the Sphere Spacing Error

```

% -- Script to run the functions sphereFit, radial_error and minimization
% in order to find the best fit for the sphere --

% This initial part of the code was retrieved from the help page of Matlab.
% The code "How can I process a sequence of files?" Can be found under this
% link <http://matlab.wikia.com/wiki/FAQ>.

% Specify the location of the files
myFolder='/Users/Alex/Caro_thesis/Matlab_code_correct/Sphere spacing error';

%Check if the folder really exists
if ~isdir(myFolder)
    errorMessage = sprintf('Error: The following folder does not exists:\n%s', myFolder);
    uiwait (warndlg(errorMessage));

```

```

    return;
end

% Get a list of the files with the same pattern
filePattern =fullfile(myFolder, '*.csv'); %if I have a mat file proceed as in *
theFiles= dir(filePattern);
for k=1:length(theFiles)
    baseFileName=theFiles(k).name;
    fullFileName=fullfile(myFolder,baseFileName);
    fprintf(1, 'Now reading %s\n', fullFileName);
    File=load(baseFileName);
    data=File;

    %Calling the sphereFit function
    [t(k), u(k),v(k), r(k)]=sphereFit(data);
    fprintf('The initial estimative for the radius is = %2.10f\n', r(k))
    fprintf('The initial estimative for the center is = %2.10f %2.10f %2.10f\n', t(k),
u(k),v(k))

    %Calling the radial_error function
    [output, SD]= radial_error(data);
    outputName =strcat('output', num2str(k), '.mat');
    save(outputName, 'output');

    %Calling the minimization function
    [a(k),b(k),c(k), Radius(k),di]= minimization(output);
    fprintf('The minimized radius is = %2.10f\n ',Radius(k))
    fprintf('The minimized center is = %2.10f %2.10f %2.10f\n',a(k),b(k),c(k));
    RadialerrorName =strcat('Radialerror', num2str(k), '.mat');
    save(RadialerrorName, 'di');

end

% Saving the minimized values
save('Radius.mat', 'Radius');
save('a.mat', 'a');
save('b.mat', 'b');
save('c.mat', 'c');

% Calculating the distance between the center of the spheres for the SD
L=[];
SD_v=[];
for i = 1:2:length(a)
    L(i)= sqrt((a(i)-a(i+1))^2+(b(i)-b(i+1))^2+(c(i)-c(i+1))^2);
    SD_v(i)= L(i)-0.16;%0.29 once is the calibrated length
end
dist=L(L~=0);
SD_pos=SD_v(SD_v~=0);%to remove the zeros from our dist matrix
save('dist.mat', 'dist');
save('SD_pos.mat', 'SD_pos');
csvwrite('L_SD_pos.csv',SD_pos);

%Calculating the mean Sphere Distance Error and std of the mean
SD = mean(SD_pos);
save('SD.mat', 'SD');
csvwrite('L_SD.csv', SD);

std_pos=std(SD_pos);
STD_mean=std_pos./(sqrt(3)); %3 = number of measured positions

save('STD_mean.mat', 'STD_mean');
csvwrite('L_STD_mean.csv',STD_mean);

MPE = 0.0001;
U =1.3072745184798300e-05;
%Assessing the values

```

```

S=[];
for i=1:length(SD_pos(:))
    if (abs(SD_pos(i))<= abs(MPE-U))
        S(i)=1;
    else
        S(i)=0;
    end
end;
end;

```

➤ Script to extract the Probing Error Form and Size

```

[...]

% Saving the minimized values

save('Radius.mat', 'Radius');

save('a.mat', 'a');

save('b.mat', 'b');

save('c.mat', 'c');

% %Calculating inout for PF

fls = dir('Radialerror*.mat');

for i=1:length(flс)

    %Loading the files

    File = load (fls(i).name); %the file is a struct

    struct=File;

    CellArray =struct2cell(struct); %conversion of struct to cell

    File = cell2mat(CellArray); %conversion from cell array to ordinary array

    data =File;

    %Calculating the standard deviation of each data

    PF_std(i) = std (data);

end

A=[];

MPE = 0.0001;

U =1.37044700736657e-5;

%Assessing the values

for i=1:length(PF_std)

```

```

    if (abs(PF_std(i)) <= (abs(MPE-U)))
        A(i)=1;
    else
        A(i)=0;
    end
end

save('PF_std.mat', 'PF_std');
csvwrite('L_PF_std.csv', PF_std);
% save('PF_pos.mat', 'PF_pos');
% csvwrite('L_PF_pos.csv', PF_pos);
%Mean value for the PF
PF=mean(PF_std)
save('PF.mat', 'PF');
csvwrite('L_PF.csv', PF);
PF_std_mean=mean(PF_std);
save('PF_std_mean.mat', 'PF_std_mean');
csvwrite('L_PF_std_mean.csv', PF_std_mean);
%Calculating the Probing Error Shape (PS)
%Necessary diameter and calibrated sphere
Diameter= 2.*Radius;
for i=1:length(Radius)
    PS_pos(i)=Diameter(i)-0.038;
end
save('PS_pos.mat', 'PS_pos');
csvwrite('L_PS_pos.csv', PS_pos);
PS= mean(PS_pos);
save('PS.mat', 'PS');
csvwrite('L_PS.csv', PS);

```

```

std_pos=std(Diameter);

Std_mean=std_pos/(sqrt(3)); %3 = number of measured probing error

save('Std_mean.mat', 'Std_mean');

csvwrite('L_Std_mean.csv',Std_mean);

B=[];

%Assessing the values

for i=1:length(PS_pos)

    if (abs(PS_pos(i))<= (abs(MPE-U)))

        B(i)=1;

    else

        B(i)=0;

    end

end

end

```

C Accuracy analysis – evaluated scan systems

a. Accuracy analysis – Laser Line Scanner System

Probing Error - Laser Line System		
	Measured Diameter (mm)	Radial error std (µm)
Pos. 1	73.9	86.5
Pos. 2	71.8	229.1
Pos. 3	71.6	190.5
Mean Diameter	72.4	
STD* (µm)	757.5	

Probing Error - Laser Line System	
	Measured Distance (mm)
Pos. 1	289.9
Pos. 2	289.3
Pos. 3	289.3
Mean Distance	289.5
STD* (µm)	207.1

Probing Error - Laser Line System					
	PF evaluation (µm)	PS evaluation (µm)	MPE - U (µm)	SD evaluation (µm)	[MPE] - U
Pos. 1	86.5	3938.5	4981.0	-78.0	4984.9
Pos. 2	229.1	1799.3		-661.6	
Pos. 3	190.5	1552.9		-730.9	

Assessment Test - Laser Line System			
	SD evaluation (µm)	E evaluation (µm)	[MPE] - U
Pos. 1	-78.0	3947,0	4984,9
Pos. 2	-661.6	1366,8	
Pos. 3	-730.9	1012,5	

* STD = Standard deviation of the mean

b. Accuracy analysis– Photogrammetric System I

Probing Error - Nikon D610 with AF-S Nikkor 50mm lens		
	Measured Diameter (mm)	Radial error std (µm)
Pos. 1	70.5	435.5
Pos. 2	70.2	456.8
Pos. 3	70.7	309.0
Mean Diameter	70.5	
STD* (µm)	132.0	

*STD = Standard deviation of the mean

Sphere Spacing Error - Nikon D610 with AF-S Nikkor 50mm lens	
	Measured Distance (mm)
Pos. 1	290.2
Pos. 2	290.2
Pos. 3	290.1
Mean distance	290.2
STD* (µm)	40.5

Assessment Test - Nikon D610 with AF-S Nikkor 50mm lens			
	PF evaluation (µm)	PS evaluation (µm)	MPE - U (µm)
Pos. 1	435.5	489.8	473.1
Pos. 2	456.8	242.2	
Pos. 3	309.0	698.9	

Assessment Test - Nikon D610 with AF-S Nikkor 50mm lens			
	SD evaluation (µm)	E evaluation (µm)	MPE - U
Pos. 1	191.7	1117.0	469.8
Pos. 2	240.3	939.2	
Pos. 3	102.0	1109.9	

* STD = Standard deviation of the mean

c. Accuracy analysis – Photogrammetric System II

Probing Error - Canon 5DSr + Canon 100mm lens		
	Measured Diameter (mm)	Radial error std (µm)
Pos. 1	38.1	7.1
Pos. 2	38.0	19.9
Pos. 3	38.1	13.5
Mean Diameter	38.1	
STD* (µm)	30.1	

Sphere Spacing Error - Canon 5DSr + Canon 100mm lens	
	Measured Distance (mm)
Pos. 1	159.9
Pos. 2	160.4
Pos. 3	160.0
Mean distance	160.1
STD* (µm)	152.2

Assessment Test - Canon 5DSr + Canon 100mm lens			
	PF evaluation (µm)	PS evaluation (µm)	MPE - U (µm)
Pos. 1	7.1	97.7	122.6
Pos. 2	19.9	7.0	
Pos. 3	13.5	97.0	

Assessment Test - Canon 5DSr + Canon 100mm lens			
	SD evaluation (µm)	E evaluation (µm)	MPE - U
Pos. 1	-107.2	-16.5	123.9
Pos. 2	419.3	446.3	
Pos. 3	33.0	244.8	

* STD = Standard deviation of the mean

D Measurement uncertainty analysis

a. Uncertainty Budget – Laser Line Scanner System

Uncertainty Laser Line Scanner - Probing Error From					
Uncertainty Source	Standard uncertainty	Type	Distribution	Units	DOF
Probing Error Form	168.7	A	Normal	μm	2
Mechanical coordinates of the robot	57.7	B	Rectangular	μm	infinity
Test procedure	19.0	B(ISO)	Normal	μm	infinity
Combined standard uncertainty (u)				179.3	
Expanded uncertainty (95%) - k=4,3				771.1	

Uncertainty Laser Line Scanner - Probing Error Size					
Uncertainty Source	Standard uncertainty	Type	Distribution	Units	DOF
Probing Error Size	757.5	A	Normal	μm	2
Mechanical coordinates of the robot	57.7	B	Rectangular	μm	infinity
Test procedure	19.0	B(ISO)	Normal	μm	infinity
Combined standard uncertainty (u)				759.9	
Expanded uncertainty (95%) - k=4,3				3267.6	

Uncertainty Laser Line Scanner - Sphere Spacing Error					
Uncertainty Source	Standard uncertainty	Type	Distribution	Units	DOF
Sphere Spacing Error	207.1	A	Normal	μm	2
Mechanical coordinates of the robot	57.7	B	Rectangular	μm	infinity
Test procedure	15.1	B(ISO)	Normal	μm	infinity
Combined standard uncertainty (u)				215.5	
Expanded uncertainty (95%) - k=4,3				926.6	

b. Uncertainty Budget – Photogrammetric System I

Nikon D610 with AF-S Nikkor 50mm lens - Probing Error Form					
Uncertainty Source	Standard uncertainty	Type	Distribution	Units	DOF
Probing Error Form	400.4	A	Normal	µm	2
Targets uncertainty	14.4	B	Rectangular	µm	infinity
Test procedure	19.0	B(ISO)	Normal	µm	infinity
Combined standard uncertainty (u)				401.1	
Expanded uncertainty (95%) - k=4,3				1724.9	

Nikon D610 with AF-S Nikkor 50mm lens - Probing Error Size					
Uncertainty Source	Standard uncertainty	Type	Distribution	Units	DOF
Probing Error Size	132.0	A	Normal	µm	2
Targets uncertainty	14.4	B	Rectangular	µm	infinity
Test procedure	19.0	B(ISO)	Normal	µm	infinity
Combined standard uncertainty (u)				134.1	
Expanded uncertainty (95%) - k=4,3				576.8	

Nikon D610 with AF-S Nikkor 50mm lens - Sphere Spacing Error					
Uncertainty Source	Standard uncertainty	Type	Distribution	Units	DOF
Sphere Spacing Error	40.5	A	Normal	µm	2
Targets uncertainty	14.4	B	Rectangular	µm	infinity
Test procedure	15.1	B(ISO)	Normal	µm	infinity
Combined standard uncertainty (u)				45.6	
Expanded uncertainty (95%) - k=4,3				196.0	

c. Uncertainty Budget – Photogrammetric System II

Uncertainty Canon 5DSr + Canon 100mm lens - Probing Error Form					
Uncertainty Source	Standard uncertainty	Type	Distribution	Units	DOF
Probing Error Form	13.5	A	Normal	μm	2
Targets uncertainty	8.7	B	Rectangular	μm	infinity
Test procedure	13.7	B	Normal	μm	infinity
Combined standard uncertainty (u)					21.1
Expandend uncertainty (95%) - k=2					42.2

Uncertainty Canon 5DSr + Canon 100mm lens - Probing Error Size					
Uncertainty Source	Standard uncertainty	Type	Distribution	Units	DOF
Probing Error Size	30.1	A	Normal	μm	2
Targets uncertainty	8.7	B	Rectangular	μm	infinity
Test procedure	13.7	B	Normal	μm	infinity
Combined standard uncertainty (u)					34.2
Expandend uncertainty (95%) - k=3					102.6

Uncertainty Canon 5DSr + Canon 100mm lens – Sphere Spacing Error					
Uncertainty Source	Standard uncertainty	Type	Distribution	Units	DOF
Sphere Spacing Error	152.2	A	Normal	μm	2
Targets uncertainty	8.7	B	Rectangular	μm	infinity
Test procedure	13.1	B(ISO)	Normal	μm	infinity
Combined standard uncertainty (u)					153.0
Expandend uncertainty (95%) - k=3,57					546.1